Geochemistry Geophysics Geosystems G3
AN ELECTRONIC JOURNAL OF THE EARTH SCIENCES
Published by AGU and the Geochemical Society

Article
Volume 9, Number 5
23 May 2008
Q05019, doi:10.1029/2007GC001886
ISSN: 1525-2027

Lithospheric dismemberment and magmatic processes of the Great Basin–Colorado Plateau transition, Utah, implied from magnetotellurics

Philip E. Wannamaker
Energy and Geoscience Institute, University of Utah, 423 Wakara Way, Suite 300, Salt Lake City, Utah 84108, USA (pewanna@egi.utah.edu)

Derrick P. Hasterok
Department of Geology and Geophysics, University of Utah, 717 W. B. Browning Building, Salt Lake City, Utah 84112, USA (dhasterok@gmail.com)

Jeffery M. Johnston
Geometrics, Inc., 2190 Fortune Drive, San Jose, California 95131, USA (jeff@mail.geometrics.com)

John A. Stodt
Numeric Resources, Inc., 1740 Kensington Avenue, Salt Lake City, Utah 84108, USA (jstodt@numericresources.com)

Darrell B. Hall and Timothy L. Sodergren
Department of Geology and Geophysics, University of Utah, 717 W. B. Browning Building, Salt Lake City, Utah 84112, USA (fractal_art@yahoo.com; timsoder@yahoo.com)

Louise Pellerin
Green Engineering Inc., 2215 Curtis Street, Berkeley, California 94702, USA (pellerin@ak.net)

Virginie Maris
Department of Geology and Geophysics, University of Utah, 717 W. B. Browning Building, Salt Lake City, Utah 84112, USA (vmaris@egi.utah.edu)

William M. Doerner
SourceOne Geophysical Inc., 10511 Golden Pines Road, Truckee, California 96161, USA (billdoerner@cs.com)

Kim A. Groenewold
Department of Geology and Geophysics, University of Utah, 717 W. B. Browning Building, Salt Lake City, Utah 84112, USA (groenewd@water.nv.gov)

Martyn J. Unsworth
Department of Physics, University of Alberta, Edmonton, Alberta, Canada T6G 2J1 (unsworth@phys.ualberta.ca)

[1] To illuminate rifting processes across the Transition Zone between the extensional Great Basin and stable Colorado Plateau interior, we collected an east-west profile of 117 wideband and 30 long-period magnetotelluric (MT) soundings along latitude 38.5°N from southeastern Nevada across Utah to the Colorado border. Regularized two-dimensional inversion shows a strong lower crustal conductor below the Great Basin and its Transition Zone in the 15–35 km depth range interpreted as reflecting modern basaltic underplating, hybridization, and hydrothermal fluid release. This structure explains most of the

geomagnetic variation anomaly in the region first measured in the late 1960s. Hence, the Transition Zone, while historically included with the Colorado Plateau physiographically, possesses a deep thermal regime and tectonic activity like that of the Great Basin. The deep crustal conductor is consistent with a rheological profile of a brittle upper crust over a weak lower crust, in turn on a stronger upper mantle (jelly sandwich model). Under the incipiently faulted Transition Zone, the conductor implies a vertically nonuniform mode of extension resembling early stages of continental margin formation. Colorado Plateau lithosphere begins sharply below the western boundary of Capitol Reef National Park as a resistive keel in the deep crust and upper mantle, with only a thin and weak Moho-level crustal conductor near 45 km depth. Several narrow, steep conductors connect conductive lower crust with major surface faulting, some including modern geothermal systems, and in the context of other Great Basin MT surveying suggest connections between deep magma-sourced fluids and the upper crustal meteoric regime. The MT data also suggest anisotropically interconnected melt over a broad zone in the upper mantle of the eastern Great Basin which has supplied magma to the lower crust, consistent with extensional mantle melting models and local shear wave splitting observations. We support a hypothesis that the Transition Zone location and geometry ultimately reflect the middle Proterozoic suturing between the stronger Yavapai lithosphere to the east and the somewhat weaker Mojave terrane to the west. We conclude that strength heterogeneity is the primary control on locus of deformation across the Transition Zone, with modulating force components.

Components: 23,891 words, 14 figures.

Keywords: magnetotellurics; Great Basin; Colorado Plateau; magmatism; extension; hydrothermal.

Index Terms: 8109 Tectonophysics: Continental tectonics: extensional (0905); 1515 Geomagnetism and Paleomagnetism: Geomagnetic induction; 8424 Volcanology: Hydrothermal systems (0450, 1034, 3017, 3616, 4832, 8135).

Received 9 November 2007; **Revised** 12 March 2008; **Accepted** 2 April 2008; **Published** 23 May 2008.

Wannamaker, P. E., et al. (2008), Lithospheric dismemberment and magmatic processes of the Great Basin–Colorado Plateau transition, Utah, implied from magnetotellurics, *Geochem. Geophys. Geosyst.*, *9*, Q05019, doi:10.1029/2007GC001886.

1. Introduction

[2] Continental rifting can be responsible for large earthquakes, sedimentary basin development and, in the extreme case, breakup of continents to form new ocean basins. The structural, magmatic and hydrothermal events that take place spawn important hydrocarbon, geothermal and mineral resources. One of the most complicated aspects of the process is the transition from active rifting to a stable bounding platform, where the interplay between tectonic forces and inherited structure could be strong. A prominent example of such a transition is that from the Great Basin to the Colorado Plateau (GB-CP) in Utah [*Eaton et al.*, 1978; *Smith et al.*, 1989; *Humphreys and Dueker*, 1994; *Wannamaker et al.*, 2001]. The interface between these provinces comprises an uplifted rift shoulder (the Wasatch Front and southward extension) heralding the 100 km-wide Transition Zone (TZ), possessing characteristics of both provinces.

[3] Three principal issues about continental extension have emerged in our study of the region. First, current understanding about the relative roles of force versus strength heterogeneity for shaping the GB-CP transition has remained ambiguous [*Sonder and Jones*, 1999]. Second, the operative process of lithospheric destruction is largely cryptic to the surface, and may range from quasi-uniform gravitational collapse of overthickened crust, to rifting that is highly nonuniform vertically and nonsymmetric laterally [*Ruppel*, 1995; *Axen et al.*, 1998]. Third, magmatism and active extension go hand in hand in the continental lithosphere. As we discuss, tentative evidence exists for enhanced melting processes in the upper mantle similar to those of volcanic continent-ocean margins [*Korenaga et al.*, 2002; *Gernigon et al.*, 2006].

[4] Electrical resistivity is a unique indicator of thermal, fluid and magmatic processes at depth [*Haak and Hutton*, 1986; *Wannamaker and Hohmann*, 1991; *Jones*, 1992, 1999; *Wannamaker*, 2000, 2005]. Since rheology is affected profoundly by temperature and the presence of fluids/melts [*Karato and Wenk*, 2002], high electrical conductivity may be an indication of weak zones in the

lithosphere where deformation can concentrate. To improve insight on extensional processes and physical state below the Great Basin (GB) to Colorado Plateau (CP), we have collected a dense, high-quality transect of magnetotelluric (MT) observations ~450 km in length from southeastern Nevada across Utah to the Colorado border (Figure 1). Data of bandwidth $>10^{+6}$ in wave period sense resistivity structure over depths of order 100 m to 250 km. Thus, MT data allow broad views of the rift process, from melting of mantle source regions, through lower crustal underplating and intrusion, to brittle regime deformational response.

2. Geological Background to the Eastern Great Basin and Colorado Plateau Region

[5] The eastern Great Basin and the Colorado Plateau have distinct geologic histories at least since middle Proterozoic time. Transition Zone (TZ) characteristics of the modern regime have evolved largely since Oligocene time, but our data will show that the long-lived contrast likely exerts control on current activity.

2.1. Pre–Great Basin Tectonic Heritage

[6] The Phanerozoic Great Basin setting was a west-facing, Atlantic-style passive margin, with a Late Proterozoic-Devonian miogeoclinal section thickening westward to nearly 15 km over rifted, Middle Proterozoic crystalline basement [*Stewart*, 1980; *Speed et al.*, 1988; *Hintze*, 1988; *Burchfiel et al.*, 1992; *Van Schmus et al.*, 1993] (Figure 2a). By contrast, the Colorado Plateau to the east accumulated relatively thin cratonal sedimentary cover near sea level [*Spencer*, 1996], with 3–4 km thickness remaining today. The basement transition between provinces roughly coincides with the Middle Proterozoic terrane suturing of Mojavia (2.0–2.3 Ga) on the west with the Yavapai domain (1.7–1.85 Ga) on the east [*Karlstrom et al.*, 1999, 2001; *Lee et al.*, 2001]. The join is far from knife-edge, but rather an intermixing of the two basement types laterally over a distance of 100 km or more [*Coleman and Walker*, 1992; *Duebendorfer et al.*, 2006]. Late Paleozoic intracontinental deformation reactivated Precambrian basement trends causing broad uplifts and basin accumulations [*Hintze*, 1988; *Dickinson and Lawton*, 2003] (Figure 2b).

[7] The Late Mesozoic, Sevier fold and thrust event driven by subduction from the west is expressed in our field area as the Canyon Range-Wah Wah-Gass Peak and the Pavant-Blue Mountains-Muddy Mountains systems [*Armstrong*, 1968, 1982; *Allmendinger*, 1992; *DeCelles*, 2004; *DeCelles and Coogan*, 2006] (Figures 1 and 2c). Mostly cryptic to the surface and detected in petroleum exploration wells in the central Utah TZ are other near-horizontal decollements (e.g., Gunnison thrust) younger than and frontal to the Pavant system [*DeCelles and Coogan*, 2006; *Johnson et al.*, 2007; *Schelling et al.*, 2007]. The related but slightly lagging, thick-skinned Laramide (Late Cretaceous-Early Eocene) compression caused gentle, broad-wavelength monoclinal uplifts in the Colorado Plateau [*Armstrong and Ward*, 1991; *Dumitru et al.*, 1991; *Miller et al.*, 1992]. Erosion of the Sevier highland over Nevada and western Utah produced the Cretaceous sedimentary foredeep several kilometers thick directly to the east in the TZ [*Hintze*, 1988; *Royse*, 1993].

[8] Regional calc-alkaline magmatism and metamorphic core complex development swept from the northernmost U.S. to the southern Great Basin over middle Eocene to early Miocene time [*Armstrong and Ward*, 1991; *Christiansen and Yeats*, 1992; *Constenius*, 1996] (Figure 2d). The sweep occurs as discrete, E-W trending belts of plutonism spanning up to 10 Ma, with intervening gaps (e.g., the "Mid-Utah magmatic gap" [*Stewart et al.*, 1977]). Most source material for this plutonism was derived primarily from the Proterozoic mantle lithosphere or lower crust [e.g., *Coleman and Walker*, 1992; *Hawkesworth et al.*, 1995; *Riciputi et al.*, 1995], possibly heated by upwelled asthenosphere during sinking of the Farallon Plate [*Perry et al.*, 1993; *Humphreys*, 1995]. Our study area is underlain by the late Oligocene-early Miocene composite plutonic belt composed of the Reno-Pioche-Marysvale-Henry-San Juan fields, the only such belt defined to penetrate the nonextended CP [*Stewart et al.*, 1977; *Nelson and Davidson*, 1993; *Rowley et al.*, 1998]. The belt is bounded sharply to the north across the E-W trending Cove Fort transverse zone, and intrusive volumes diminish to the south across the Blue Ribbon zone [*Rowley et al.*, 1998].

2.2. Miocene to Present Extensional Regime

[9] Fission track (FT) and Ar/Ar geochronology integrated with extensive geologic mapping show that Great Basin exhumation was essentially complete by early middle Miocene time, with most active extension becoming concentrated along its

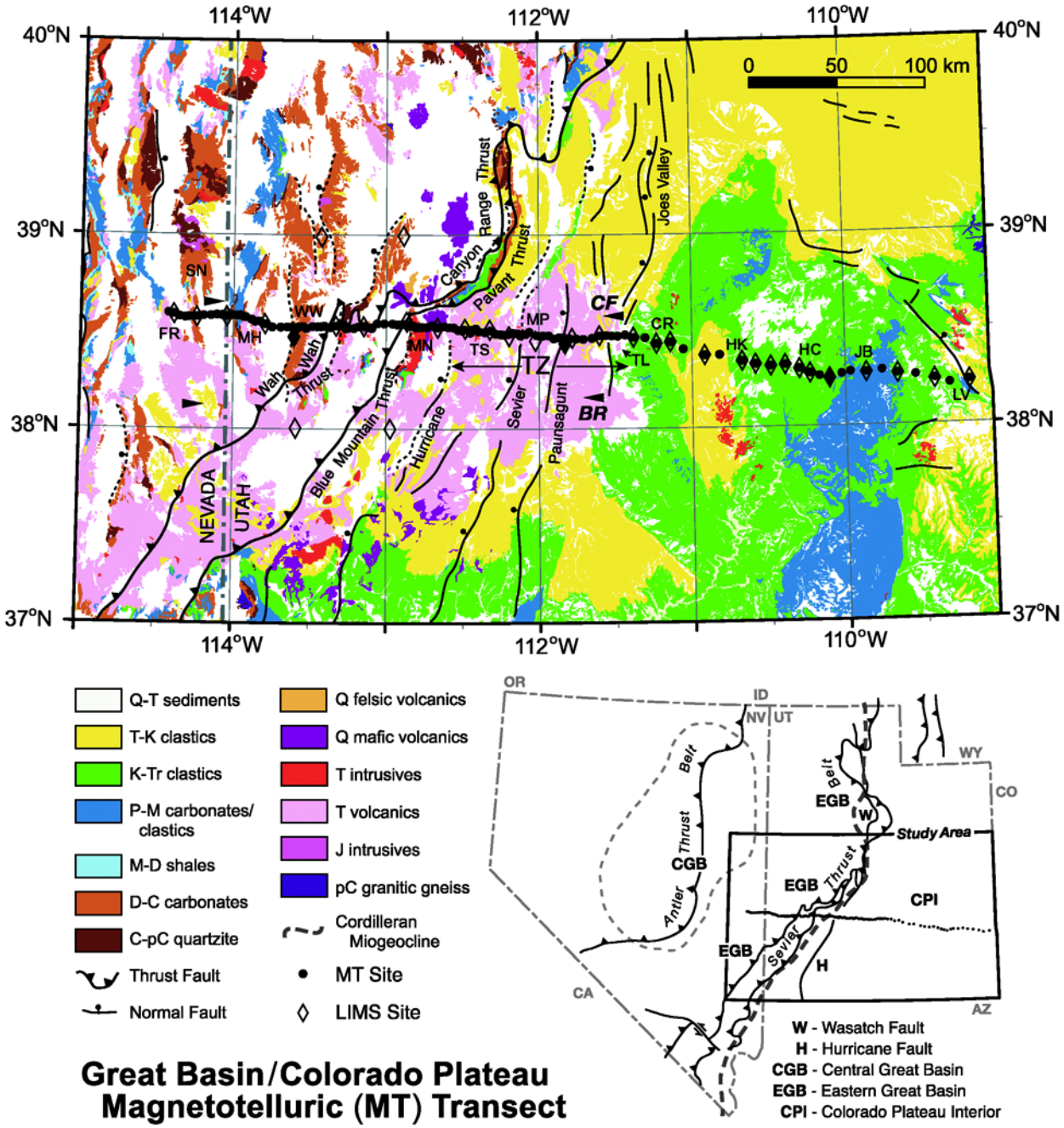

Figure 1. Geologic map of central Utah and easternmost Nevada across the eastern Great Basin (GB) and Colorado Plateau (CP) interior, from state survey online sources. GB-CP Transition Zone (TZ) is the ~100 km wide, N-S trending swath in west central Utah showing incipient normal faulting. There are 117 MT wideband (solid circles) and 34 long-period sites (lozenges, solid for 1-year occupations) in the campaign. Major Sevier-era thrust and late Tertiary normal faults are labeled. The Hurricane normal fault scarp is usually assigned as the southern extension of the Wasatch Front. Other labeled physiography includes Snake Range (SN), Fortification Range (FR), Mountain Home Range (MH), Wah Wah Mountains (WW), Mineral Range (MN), Tushar Mountains (TS), Marysvale Peak (MP), Thousand Lake Mountain (TL), Capital Reef (CR), Hanksville (HK), Horseshoe Canyon (HC), Junction Butte (JB), and Lisbon Valley (LV). Elongate horizontal black arrowheads denote Cove Fort (CF) and Blue Ribbon (BR) transverse zones bounding the E-W Pioche-Marysvale igneous belt.

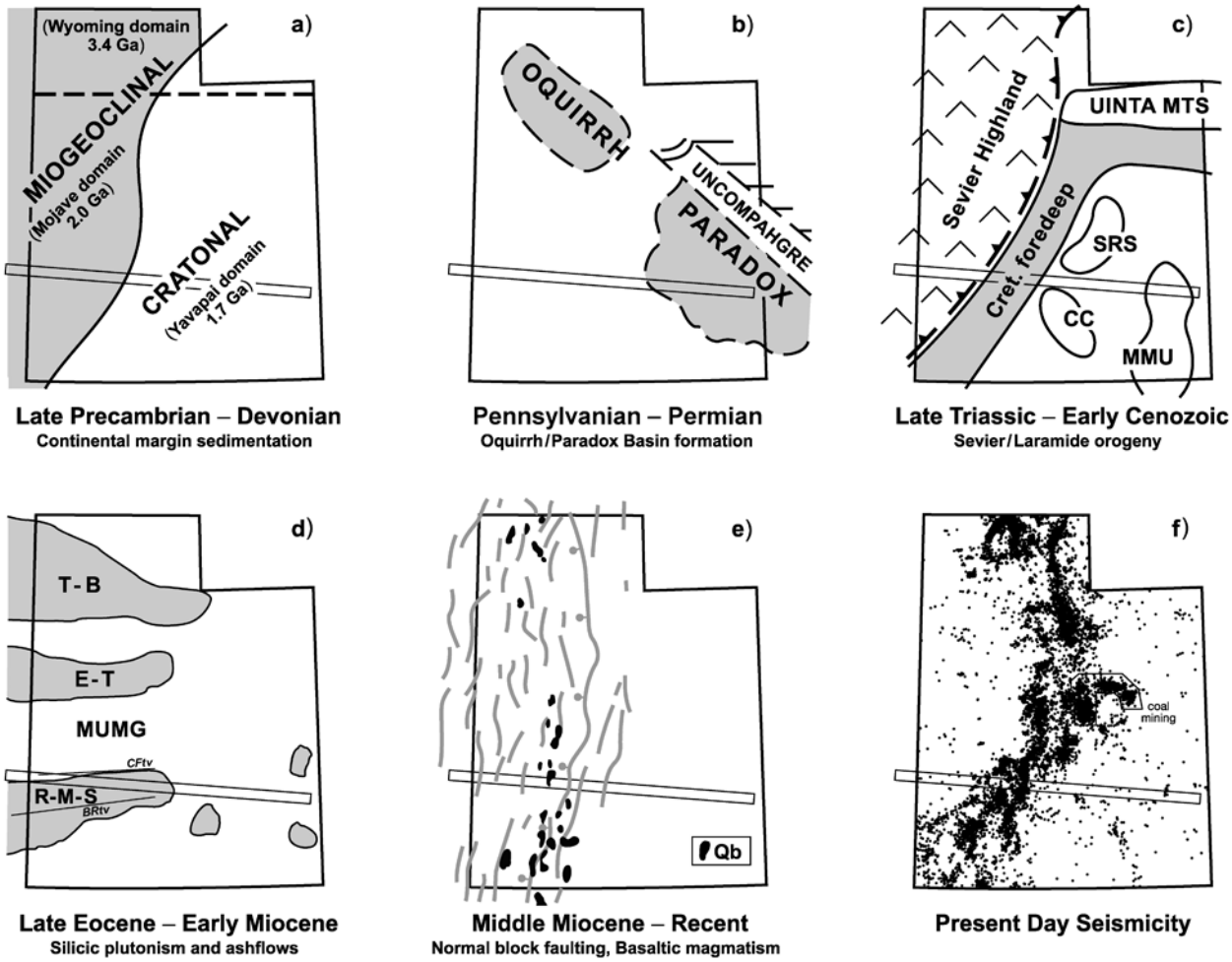

Figure 2. Principal stages in geological evolution of the Great Basin–Colorado Plateau transition since formation of the Precambrian crystalline basement. In Figure 2a, a major rift margin formation event provided setting for miogeoclinal section of quartzite under carbonate extending west to central Nevada. In Figure 2b, Paleozoic intracontinental deformation exploited Precambrian weaknesses, causing uplift and basin formation. In Figure 2c, collision of the Sierra Nevada to the west doubled crustal thicknesses of the Sevier highland and emplaced massive thin-skinned thrust sheets with toes lying across our study. In the CP, this was expressed as thick-skinned monoclines including the San Raphael Swell, Circle Cliffs, and Monument Uplift. In Figure 2d, predominantly east-west belts of granodioritic plutons crossed western Utah including our study. These include the Tuscarora-Bingham, Eureka-Tintic, and Reno-Marysvale-San Juan belts, with the latter two separated by the Mid-Utah magmatic gap (MUMG). In Figure 2e, regional extension widened the Great Basin and emplaced a north-south trend of Quaternary magmatism the length of the state. In Figure 2f is plotted present-day seismicity of the Utah Transition Zone, provided by W. Arabasz. MT transect denoted with east-west open bar. Panels based on *Hintze* [1980, 1988], *Stewart* [1980], *Stewart et al.* [1977], *Christiansen and McKee* [1978], *Christiansen and Yeats* [1992], *Dickinson and Lawton* [2003], and *Arabasz et al.* [2007].

eastern and western margins [*Christiansen and Yeats*, 1992; *Wernicke*, 1992; *Miller et al.*, 1999; *Dumitru et al.*, 2000; *Stockli et al.*, 2001; *Wannamaker et al.*, 2001] (Figure 2e). Nonplutonic areas of the eastern Great Basin are rifted by relatively few, large-displacement normal faults that define longitudinally continuous ranges and basins, whereas the E-W trending plutonic belts exhibit a larger number of geometrically diverse, smaller-displacement faults [*Coleman et al.*, 1997]. Neither the well-known Sevier Desert Reflector (regardless of its cause) nor the east-dipping, Snake Range low-angle decollement controlling most of that core-complex uplift have clear expression in our plutonic terrain [*Smith et al.*, 1989; *Miller et al.*, 1999; *Wills et al.*, 2005; *DeCelles and Coogan*, 2006].

[10] TZ deformation apparently started distinctly later than the main GB phase of exhumation. The Mineral Range on our profile uplifted ~9–10 Ma [*Nielson et al.*, 1986], even though the plutonic complex emplaced 25–17 Ma [*Coleman et al.*, 1997]. A single fission track result indicates that the main faulting between the Pavant Range and the Tushar Mountains occurred ~7 Ma [*Rowley et al.*, 1979]. On the Hurricane Fault south of our line, *Stewart and Taylor* [1996] infer motion in late Miocene or early Pliocene time on the basis of dated volcanic offsets. *Rowley et al.* [1981] date offset rhyolites in Kingston Canyon to indicate early Pliocene fault motion. In the Wasatch Plateau ~39.5°N, strikes of early Miocene potassic dikes are ~N60°W, but dikes intruded 7–8 Ma strike N-S [*Tingey et al.*, 1991] indicating a change to E-W extension by then. At Big Rock Candy Mountain in Sevier Valley, Ar/Ar age spectra show evidence of a 6.6 Ma heating event associated with uplift of the massif and downcutting by the Sevier River [*Cunningham et al.*, 2005, 2007]. Paleoelevation estimates from basalt vesicles suggest most uplift in the Marysvale area took place within 5 Ma [*Sahagian et al.*, 2002]. In southern Sevier Valley, offset tephra beds show most graben faulting there occurred later than 7 Ma [*Cunningham et al.*, 2007]. On Fish Lake plateau, a set of NNW-striking grabens formed in the 5–1 Ma time interval while the latest NNE-trending grabens including Fish Lake itself appear to have formed <1 Ma [*Bailey et al.*, 2007]. These indicators point to a latest Miocene-earliest Pliocene age for establishing the thermal regime and normal faulting of the TZ, rather than an early middle Miocene age like the Great Basin proper.

[11] Degree of surface extension in the GB-CP Transition Zone is minor (<10%) compared to the eastern Great Basin (50–100%) [*Wernicke*, 1985, 1992]. Modern seismicity, geodetic data, and young fault scarps [*Niemi et al.*, 2004; *Hammond and Thatcher*, 2004] testify to east-west uniaxial extension of a few mm/a developing across the TZ and into the eastern GB. The Intermountain Seismic Belt and Transition Zone nearly coincide in central to southwestern Utah, and seismicity appears equally active in both plutonic and nonplutonic crustal domains [*Arabasz et al.*, 2007] (Figure 2f). Most TZ focal depths are ~15 km, but on our profile there is a zone of deeper quakes (to 25 km) from Sevier Valley to beneath the Tushar Range. Some quake swarms just north of our line in the TZ are consistent with hydrothermal or magmatic fluid movement [*Arabasz et al.*, 2007].

[12] Early mafic lavas of the Great Basin were highly potassic, with trace element and isotopic signatures that indicate initial purging of low-melting point components from metasomatized mantle lithosphere [*Best et al.*, 1980; *Kempton et al.*, 1991; *Nelson and Tingey*, 1997; *DePaolo and Daley*, 2000]. The metasomatism includes both Precambrian and Laramide-age inputs [*Hawkesworth et al.*, 1995; *Thompson et al.*, 1997; *Wannamaker et al.*, 2000, 2001; *Humphreys et al.*, 2003; *Smith et al.*, 2004; *Usui et al.*, 2006]. Quaternary basalts, in contrast, occur along a N-S belt in the eastern GB, from the western Grand Canyon to the Black Rock Desert in the north (Figure 2e) and include some juvenile asthenospheric mantle contribution to magma production [*Nelson and Tingey*, 1997; *Smith et al.*, 1999; cf. *Gibson et al.*, 1993]. Deep crustal-upper mantle magmatism appears equally active under the plutonic crustal domain as the nonplutonic, as evident in the Quaternary bimodal volcanic field of the central Mineral Mountains 6–10 km south of our profile [*Nielson et al.*, 1986].

2.3. Enigmatic Geophysical Nature of the Great Basin–Colorado Plateau Transition

[13] The Great Basin–Colorado Plateau transition shows widely ambiguous indicators of activity at the surface, represented succinctly by the end-member models of Figure 3. A primary goal of our work is to distinguish between these alternatives with MT.

[14] On the one hand, some evidence supports a mode of uniform extension versus depth beneath the transition zone (scenario in Figure 3a), such as simple gravitational collapse of warming crust [cf. *Sonder and Jones*, 1999]. For example, the degree of TZ surface extension is slight and its elevations are higher than in either the CP or the GB, consistent with it having the thickest crust of the MT profile. In the TZ to the north and south of our study area, the thickening in part may reflect a remnant sedimentary section of the Cretaceous overthrust foredeep [*Allmendinger*, 1992; *Royse*, 1993]. Under our transect, thickening may be enhanced by the mid-Miocene plutonism of the Tushar-Marysvale field [*Nelson and Davidson*, 1993; *Rowley*, 1998; *Cunningham et al.*, 2007]. *Pakiser* [1989] interprets sparse, unreversed quarry blast profiles to show the thinnest crust lying under highly extended eastern Great Basin of western

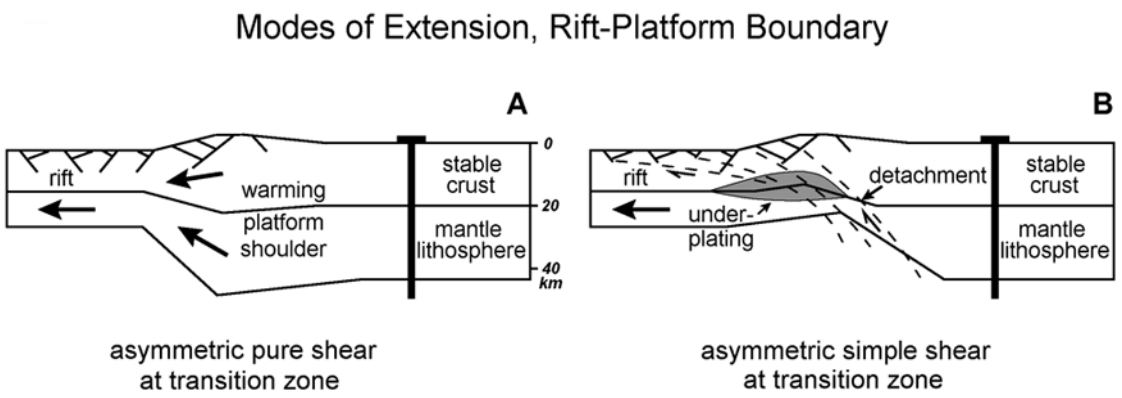

Figure 3. Possible manifestations of extensional consumption of formerly stable craton described in text. (a) Extension is fairly uniform with depth, occurring primarily by gravitational collapse of lithosphere which is thick compared to nearby extended regime. (b) Extension is in response to flow of lower crust toward extended terrane, and progressive displacement of thinning toward the platform. Mantle support of high TZ elevation is required if crust is thinned, which may include upwelling and melting.

Utah, with no thinning resolved under the TZ. *Nelson and Davidson* [1993] and *Nelson and Harris* [2001] from plutonic petrologic modeling and regional geophysics argue that mafic, stronger CP-like lower crust extends westward under the TZ making it resistant to extension. Quaternary mafic volcanism lies in a precise N-S trend passing through highly extended western Utah [*Nelson and Tingey*, 1997], not signaling mantle extension concentrated under the TZ. Finally, gravity-topography coherency analyses show effective elastic thickness (T_e) and viscosity under the TZ as retaining high, CP-like values [*Lowry et al.*, 2000].

[15] In contrast, highly nonuniform extension below the Transition Zone can be supported, perhaps a variant of the whole-lithosphere simple normal shear model of *Wernicke* [1985] (scenario in Figure 3b). *Keller et al.* [1975] and *Smith et al.* [1989] interpret the same refraction data as *Pakiser* [1989] to show that the thinnest crust lies under the western TZ and not most-extended western Utah. *Loeb and Pechmann* [1986] from two-station earthquake travel times (also unreversed) inferred very thin crust (to 23 km) of $V_P < 7$ km/s under the TZ, in turn underlain by a substantial "rift pillow" of 7.4–7.5 km/s. Receiver functions show strong mid-crustal conversions under the TZ corroborating the high V_P [*Sheehan et al.*, 1997; *Gilbert and Sheehan*, 2004]. Rift pillows would imply focused extensional processes in the mantle [*Korenaga et al.*, 2002; *Gernigon et al.*, 2006], in this case located under the TZ as well as the highly extended eastern GB. Heat flow and Curie depth of the TZ resemble those of the eastern Great Basin [*Shuey et al.*, 1973, 1977; *Bodell and Chapman*, 1982; *Wannamaker et al.*, 2001], at odds with vertically uniform extension [*McKenzie*, 1978; *Lachenbruch and Sass*, 1978]. High T_e from gravity/topography coherence would be a misleading indicator if mantle-based dynamic forces are acting.

3. Magnetotelluric Observations and Model Construction

[16] Tectonism of the southwestern United States has motivated deep electrical resistivity investigations there for over 40 years [*Gough*, 1989]. Since we have a single MT profile, as much information as possible must be obtained primarily within a two-dimensional (2-D) framework. An extensive simulation and experience base has been built up on viable approaches to resolve deep target structures in the face of nonideal geometries, aided in our case by prior regional results and key, off-profile MT data.

3.1. Early Geomagnetic Variation Array Studies

[17] Pioneering resistivity models of the GB and CP were derived by *Porath et al.* [1970] and *Porath* [1971] using magnetometer arrays recording temporal variations in the three-component vector magnetic field. Simultaneous multisite magnetovariation (MV) data allow extraction of the anomalous field component due to lateral structural changes within the Earth, most directly zones of concentrated electric current flow. Their trial-and-error forward models showed strong, north-south conductors under the GB-CP transition and the northern Rio Grande Rift of west central Colorado

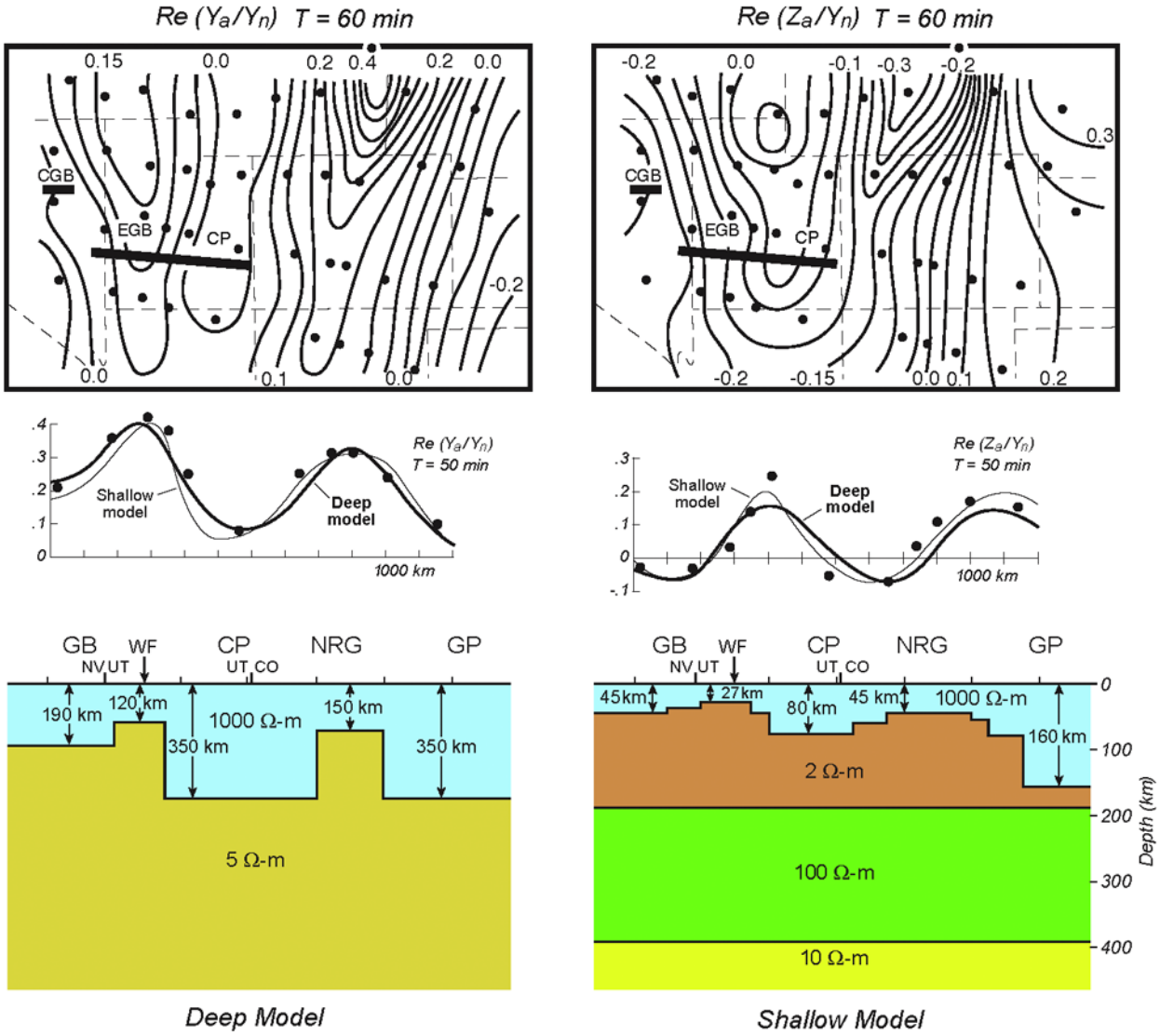

Figure 4. (top) Anomaly maps of horizontal (Y) and vertical (Z) magnetic field variations at a period of 60 min for Great Basin and Colorado Plateau regions. (middle) Anomaly profiles at 50 min period for the line of MV stations closest to our transect. Y_{ia}/Y_n refers to in-phase anomalous horizontal field normalized by external inducing field, while Z_{ia}/Y_n refers to normalized in-phase anomalous vertical field. (bottom) Alternate 2-D model views derived by trial-and-error forward fitting of MV profile data, which provide nearly equivalent fits (middle). Horizontal black rectangles are locations of modern, dense MT profiles of *Wannamaker et al.* [1997a] in the central Great Basin (CGB), plus the current profile across the eastern GB and the CP. Wasatch Front is WF. Redrawn after *Porath et al.* [1970] and *Porath* [1971].

(Figure 4). In detail, their modeling indicated that the strongest, N-S trending conductive axis in Utah centers under the southern continuation of the Wasatch Front, and not the highly extended Sevier Desert to the west. The early reconnaissance studies served as important constraints in overall geophysical models of the GB-CP transition [e.g., *Thompson and Zoback*, 1979].

[18] The MV method has relatively poor depth resolution because it does not include the electric field as in MT [*Vozoff*, 1991]. Acceptable forward models fitting the data place low-resistivity variations either near the base of the crust or deep in the upper mantle (Figure 4). However, the MV anomalies imply that the Utah and Colorado axes strike clearly N-S [*Gough*, 1989]. They do not trend NE-SW [cf. *Humphreys and Dueker*, 1994] or appear affected by possible NE magmatic alignments like the Pahranagat-San Rafael trend [*Nelson and Tingey*, 1997]. Instead they parallel the Quaternary

mafic eruptions of the Black Rock-Grand Canyon trend (Figures 1 and 2e) and the general strike of the transition. The anomalies continue to northwestern Arizona but probably stop short of the quiescent southern Basin and Range. In particular, *Porath et al.* [1970] observed a vertical H-field peak near the eastern edge of the TZ with which we can compare our data and models.

3.2. MT Transect Measurements Across the Great Basin–Colorado Plateau Transition

[19] This is a large and complex MT data collection spanning many types and scales of resistivity structure. Each structural element of Figure 2 has a discernible effect upon the MT response.

3.2.1. MT Data Collection and Processing

[20] In the MT method, natural electric (E) and magnetic (H) fields are recorded and processed to the frequency domain to estimate the 2×2 plane wave tensor impedance $\mathbf{Z}$, and the 1×2 tensor $\mathbf{K_z}$ describing the normalized vertical H-field (called the tipper) [*Vozoff*, 1991; *Simpson and Bahr*, 2005]. Over two-dimensional (2-D) structures where one of the measurement axes is parallel to geoelectric strike (x here by convention), the MT response separates into two independent modes. These are the transverse electric (TE) mode, where $E_x = Z_{xy}H_y$ and $H_z = K_{zy}H_y$ and electric current flows parallel to strike, and the transverse magnetic (TM) mode, where $E_y = Z_{yx}H_x$ and current flows perpendicular to strike. Simple arithmetic transformation of complex impedance elements to apparent resistivity (ρ_a) and impedance phase (φ) aids visual data appraisal. Data herein are displayed with a constant x axis of N15°E for all sites and all periods, consistent with geological trends and deep geoelectric axes discussed shortly.

[21] Our MT profile consists of 117 wideband (period T from 0.008 to ~500 s) and 30 long-period (20 to 10^4 s) soundings running east-west for just over 450 km (Figure 1). Profiling began in the late 1970s with 15 five-channel sites by Geotronics Corp. for geothermal exploration across the northern Mineral Range and Milford Valley. Subsequently, 53 wideband sites were taken from 1986 to 1990 with the University of Utah MT system using a local reference of two H channels [*Gamble et al.*, 1979]. Time series subsets were quality-sorted by spectral multiple coherence [*Stodt*, 1983; *Egbert and Livelybrook*, 1996]. This served well in most cases, except for sites within ~20 km of the Intermountain Power Plant DC transmission system originating north of Delta, Utah, extending southward along western Milford Valley eventually to Los Angeles. Broadband current fluctuations on this line prevented usable data over periods 0.3–10 s in the TE mode and the tipper. The TM mode was relatively unaffected due to the N-S line orientation. Across the Transition Zone and from Canyonlands National Park to the Colorado border, 49 sites were collected by Quantec Geoscience Inc. in 2004 and 2005. Robust remote referencing was cross-site [*Egbert and Booker*, 1986; *Larsen et al.*, 1996], and with the Parkfield California permanent MT observatory [*Wannamaker et al.*, 2004] for sections across regional high-tension power lines. Standard errors usually were within 4% in ρ_a, 1° φ, and 0.015 tipper (dimensionless). Average site spacing was ~3 km over the heterogeneous eastern GB, 4–5 km over the TZ and 6–10 km over the CP.

[22] The 30 long-period sites were acquired in 1999, 2004 and 2005 using LIMS instruments from the EMSOC MT facility. Sampling interval was 5 s and typical occupation times were 1–2 months. Single-site robust processing [*Jones et al.*, 1989] gave excellent long-period data due to the strong nature of signals in this band. Three sites, one in the eastern GB, one in the TZ and one in the CP, were occupied for 1 year to achieve data with phase errors under 1° at 13650 s period. Fewer long-period sites are needed than wideband because the lateral variation of the response at long periods has a much smoother frequency dependence. Standard deviations usually were within 2% for ρ_a, 0.5° φ, and 0.0075 tipper. There also are four LIMS sites off-profile, two ~50 km to the north and two ~50 km to the south in the eastern Great Basin for along-strike control (Figure 1).

3.2.2. Observed MT Pseudosections

[23] Nominal TM mode plots (Figure 5) show conductive GB graben sediments causing low-resistivity anomalies at all periods; the vertically streaked form of apparent resistivity ρ_{yx} portrays the near discontinuities in the electric field as it crosses resistivity boundaries [*Wannamaker et al.*, 1980, 1984; *Vozoff*, 1991; *Wannamaker*, 1999]. These are much subdued over the less-developed valleys of the TZ and nonexistent in the CP. Low resistivities toward longer periods spanning the Awapa Plateau overlie late Miocene lava flows and thus cannot be due to Pliocene-present graben formation, but instead likely are residual Sevier foredeep sediments. Over the Cathedral Valley to Caineville

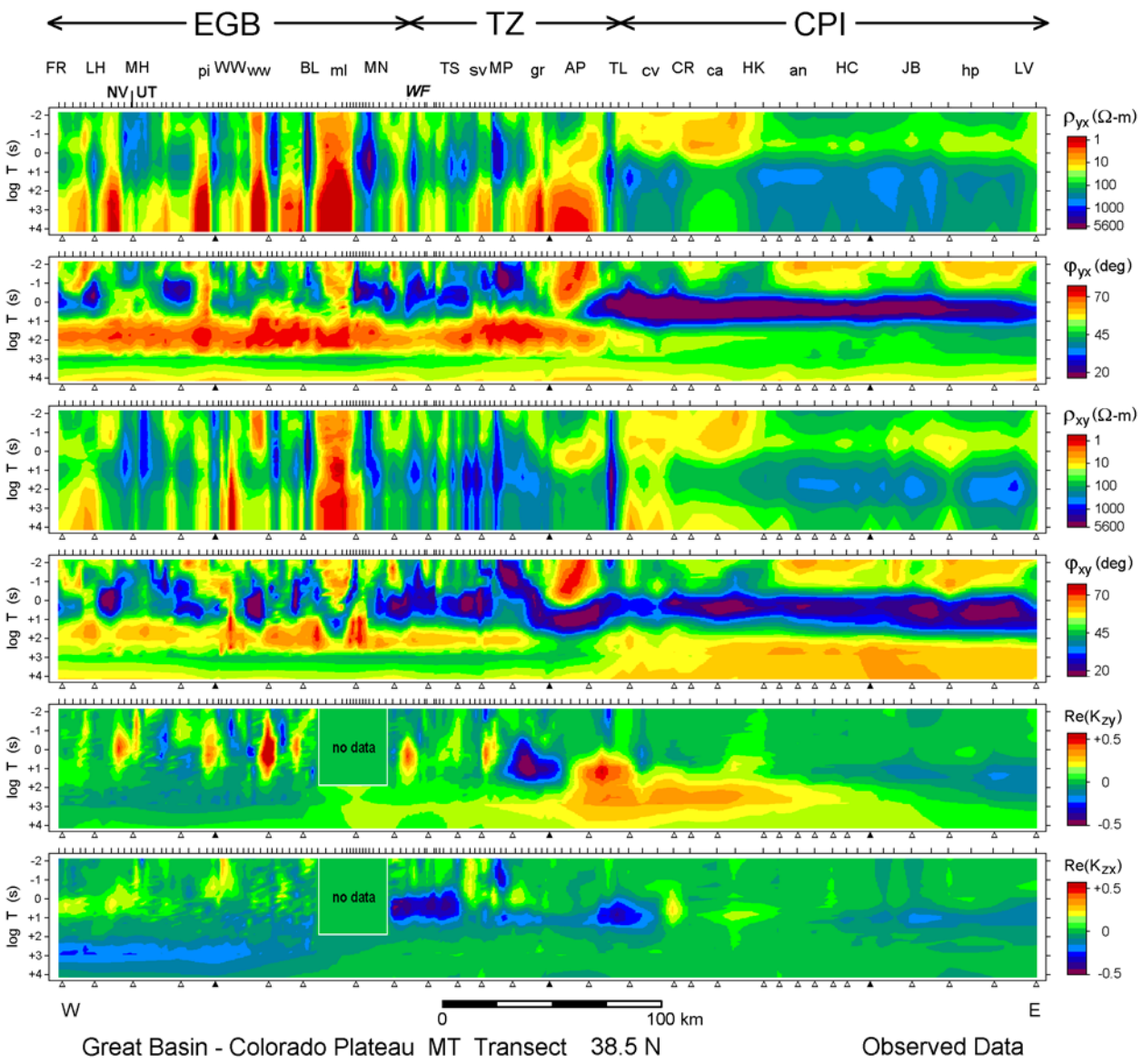

Figure 5. Pseudosections of observed MT results for merged wideband and long-period data at 117 sites on GB-CP transition profile. Log period (T, in s) serves as ordinate and horizontal distance serves as abscissa for contour plots of MT response amplitude. Quantities shown include cross-strike (TM mode) apparent resistivity and impedance phase (ρ_{yx} and ϕ_{yx}, top two panels), along-strike (TE mode) (ρ_{xy} and ϕ_{xy}, third and fourth panels), and the real part of the normalized vertical field due to along-strike and cross-strike current flow ($Re(K_{zy})$ and $Re(K_{zx})$, fifth and sixth panels). Tick marks along the top of each panel denote wideband site locations, while triangles along the bottom are long-period site locations (solid triangles are 1-year occupations). Geographic locations include Fortification Range (FR), Limestone Hills (LH), Mountain Home range (MH), Pine Valley (pi), Wah Wah Mountains (WW), Wah Wah Valley (ww), Beaver Lake Mountains (BL), Milford Valley (ml), Mineral Range (MN), Tushar Range (TS), Sevier Valley (sv), Marysvale Peak (MP), Grass Valley, (gr), Awapa Plateau (AP), Thousand Lake Mountain (TL), Cathedral Valley (cv), northern Capitol Reef Park (CR), North Caineville Mesa (NC), Hanksville (HK), Angel Point (an), Horseshoe Canyon (HC), Junction Butte (JB), Hatch Point (hp), and Lisbon Valley (LV).

interval, short-period lows in ρ_{yx} denote late Jurassic (early foredeep) Carmel-Summerville-Morrison shales. East from Hanksville, high short-period ρ_{yx} reflects resistive late Triassic-early Jurassic Navajo-Kayenta-Wingate sandstones near-surface, over low-resistivity Triassic Chinle-Moenkopi shales. Resistive Proterozoic basement at 3–4 km depth causes all ρ_{yx} values to rise for T > 1 s.

[24] The phase response of bounded objects like the grabens is band-limited, clarifying the influence

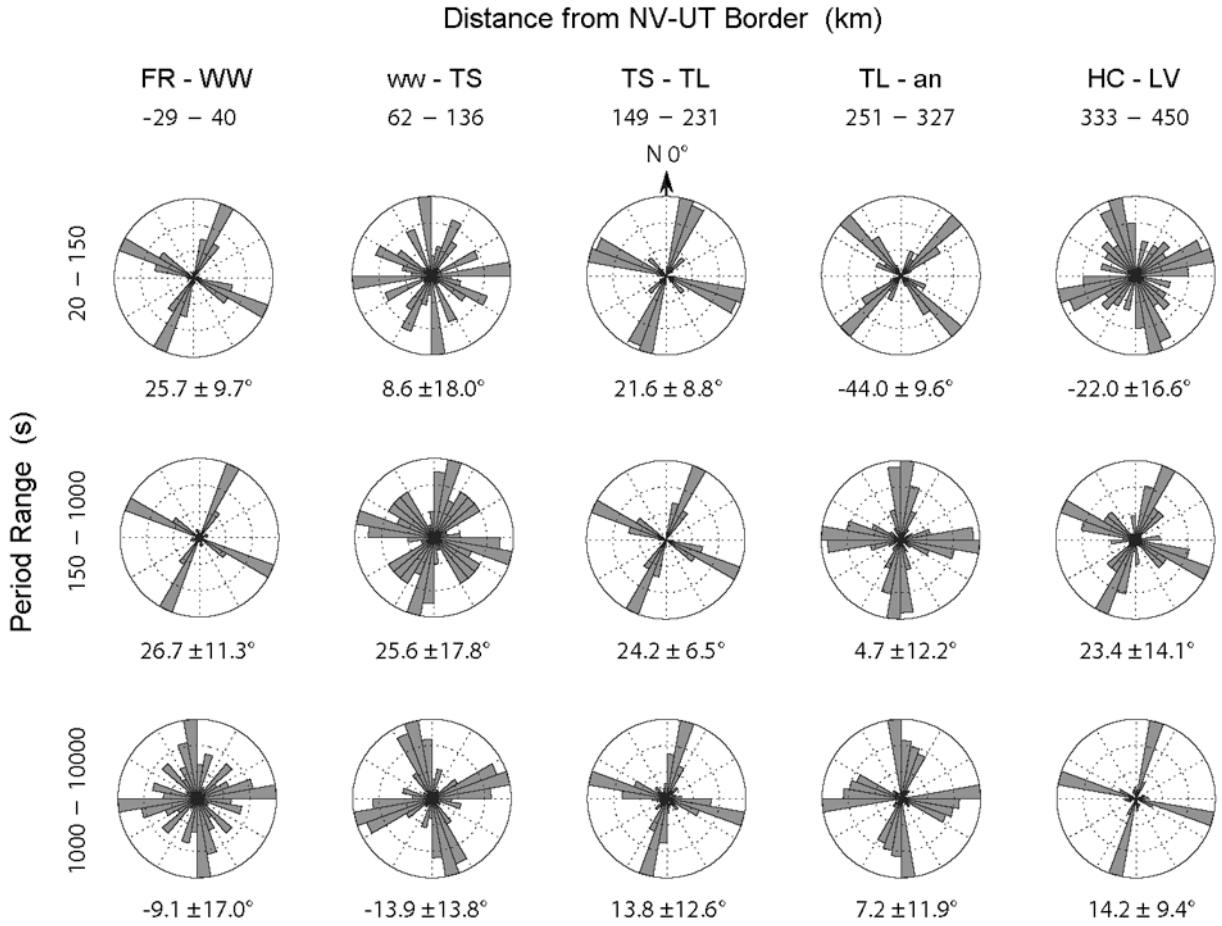

Figure 6. Phase tensor principal axes binned to 10° increments in rose histograms over three period bands for the 30 long-period (LIMS) sites on our transect. Mean direction from true north with standard deviation plotted at bottom of each rose, using statistical formulas from *Batschelet* [1981]. Geography spanned by each rose labeled according to locations in Figure 5.

of deeper, larger structures. In particular, a prominent high in φ_{yx} in the period range 10–300 s overlies the entire GB and TZ segments of the transect, ending abruptly near Thousand Lake Mountain at the eastern edge of the TZ (Figure 5). It denotes high conductivity in the lower crust of a quasi-layered disposition, and shows right from the data that a thermally active state like the GB characterizes the TZ as well. Only a weak phase high is seen across the CP, fading eastward to be essentially invisible. In the 1–10 s range, low φ_{yx} over the CP indicates its coherently resistive and thick crystalline crust, much more so than the GB or the TZ. Longer than ~500 s, φ_{yx} becomes more neutrally valued close to 45° with a final mild rise at the longest periods (>5000 s).

[25] The nominal TE (xy) mode quantities resemble the TM in showing evidence for a conductive GB and TZ lower crust and mostly resistive CP crust at middle periods. The former structure however is expressed more weakly in φ_{xy} than φ_{yx} (Figure 5). Correspondingly, much higher values of ρ_{xy} than ρ_{yx} are seen toward long periods over the entire GB-TZ interval, by on average a factor of 4–5. We show in Appendix A that this likely is caused by the Pioche-Marysvale plutonic belt under our profile acting as a narrow (20–40 km wide), resistive crustal belt running E-W across the entire eastern GB and TZ. The belt inflates the N-S electric field, thus increasing ρ_{xy} and decreasing φ_{xy} toward a static limit over the 1–1000 s range; longer-period φ_{xy} is little affected. Negligible effect upon the TM data from the belt is evident. A zone of high φ_{xy} across the CP for T > 200 s turns out to reflect the active and conductive lower crust in the TZ and GB to the west, plus more conductive GB-TZ upper mantle particularly in the N-S direction.

[26] Stripe-like anomalies of ρ_{xy} to the longest periods reveal finite strike of the grabens and other sediments we crossed, so that near-discontinuities in the E-field off-profile permeate the length of the valleys [*Wannamaker et al.*, 1980, 1984; *Wannamaker*, 1999]. The most pronounced by far is Milford Valley, but the effects are seen as well with the Cretaceous foredeep sediments under Capitol Reef Park area. They persist even with fine-tuning of the rotation angle. In a purely 2-D geometry, TE mode ρ_{xy} and φ_{xy} anomalies would be band-limited and die away toward long periods. These and other 3-D effects are the bane of 2-D interpretation of the TE mode and motivate us to take an approach emphasizing the TM which is generally less prone to end effects [*Wannamaker*, 1999].

[27] Vertical H-field element K_{zy} is that which would be interpreted in a 2-D framework (Figure 5). Several compact anomalies for T < 10 s in the eastern GB relate to the individual grabens. A strong reversal around 10 s over the Awapa Plateau is a companion response to the low ρ_{yx} and denotes a buried conductive axis. Most notably for $Re(K_{zy})$, a large positive anomaly in the 100–10000 s range extends from the Awapa Plateau eastward past Hanksville to Horseshoe Canyon at the western edge of Canyonlands National Park. This is the feature which was prominent in the vertical component of the early magnetovariational work of Porath (Figure 4). Element K_{zx} is diagnostic of departures from a purely 2-D geometry. Shorter-period, laterally variable anomalies indicate for example that the profile does not cross the grabens exactly at their centers. Negative anomalies across the TZ in the 1–10 s period range indicate the presence of more conductive material nearby to the north of our line, possibly associated with the transition from plutonic to sedimentary rocks. A notable negative in $Re(K_{zx})$ occurs at long periods (300–2000 s) over the western ~100 km of the GB segment, evidence of a crustal-scale increase in conductivity from south to north there. These are complications for a 2-D interpretation, the treatment of which we discuss later. However, for the great majority of the transect at longer periods (T > 100 s), K_{zx} is small.

3.2.3. MT Strike Indicators

[28] The assumed geoelectric strike of N15°E based largely on observed geology is tested against principal axes of the impedance phase tensor [*Caldwell et al.*, 2004] (Figure 6). The majority of the rose histograms show peaks which are ~N15°E, allowing for the 90° ambiguity in impedance, consistent with surface geological trends. Exceptions include the CP at shorter periods where the directions are more NE-SW and NW-SE on average; this result may reflect upper-middle crustal basement faulting trends controlling the Paleozoic and Mesozoic uplifts. Axes also are rather indeterminate from the San Francisco Range to the foot of the Tushar Mountains. Orientation is fairly clear across the Transition Zone itself.

[29] Trends of phase tensor axes are consistent with the vertical magnetic field responses (Figure 5). Over much of the CP for T of 10–30 s, $K_{zx} \approx K_{zy}$, confirming the N ± 45° trends. In the San Francisco Range-Tushar Mountains interval, both K_{zx} and $K_{zy} \approx 0$ so strike is indeterminate. The long-period K_{zx} anomaly over the western ~100 km of the profile implies an E-W electrical strike to a larger-scale resistivity gradient, underscoring the 90° impedance repetition and exemplifying where impedance alone with surface geology could mislead one on deep strike. Fortunately, for T > ~20 s, strike from $\mathbf{K_z}$ (tipper) clearly is near the assumed N15°E under the Transition Zone and across its eastern edge, with small values of K_{zx}.

3.3. Two-Dimensional Resistivity Inversion Models

[30] The dominant NNE grain of structure despite irregularities encourages us that most of the pertinent information content can be extracted within a 2-D modeling and inversion framework. The broad-scale 3-D effect inflating the TE impedance of the GB-TZ (Appendix A) provides a cautionary note in the MT modeling but does not fundamentally limit our data set.

3.3.1. Inversion Model Setup

[31] The main inversion code applied here is a simplified in-house implementation similar to the Occam-2 approach [*DeGroot-Hedlin and Constable*, 1990] using the forward problem of *Wannamaker et al.* [1987], the Jacobians of *Pastana de Lugão and Wannamaker* [1996], and the iterative parameter step equation of *Mackie et al.* [1988] where model slope is damped relative to that of an a priori model. The forward mesh is 573 × 70 nodes (including 10 air layers) extending to ~4000 km each side of the TZ and to total depth of 860 km. There are four element columns per MT station increasing geometrically downward from 25 m thickness at the surface. Two parameter columns per station are used, one under and one between

each site, to a depth of 660 km and to within one finite element of each side of the mesh, for a total of ~12000 parameters.

[32] The TM mode $\log_{10}(\rho_{yx})$ and φ_{yx}, TE mode φ_{xy}, and Re(K_{zy}) over 43 periods are the inverted quantities, comprising ~13000 data points, for the 2-D distribution of $\log_{10}(\rho)$ [cf. *Hohmann and Raiche*, 1988]. Error floors of 10%, 2°, and 0.015 were applied to apparent resistivity, phase and K_{zy} respectively. Floors one-half of those amplitudes were applied to the long-period LIMS data due to their greater accuracy and sparser number. Instead of sweeping through a series of roughness damping factors at each iteration, one value is selected at the outset whereby the square norm of the roughening matrix is a fraction (typically 0.2) of the norm of the error-weighted parameter sensitivity matrix, adjusted each iteration. We find this achieves a good fit with apparently stable models in a small number of iterations (~10 usually). Final normalized root-mean-square (RMS) misfits for all data sets were in the range 1.2–1.3. Trial runs with a range of damping factors 0.1–0.5 were done on final models to ensure the persistence of important areas of structure.

[33] Models derived thus were compared to 2-D inversions performed with the nonlinear conjugate gradient inversion program of *Rodi and Mackie* [2001], using similar control parameters and achieving similar fits. There were three finite difference columns per MT station, each of which was a parameter column. In nomenclature of the program documentation, trade-off parameter value (tau) was 3, which is a default value to balance fitting the MT data and generating a spatially smooth model. A horizontal-to-vertical smoothing parameter (alpha) of 3 was used to emphasize horizontal structures and a uniform degree of smoothing versus depth (beta = 0) was applied. To conserve space, we show a single comparison of the two inversions in an expanded view of TZ structure later in the paper.

[34] A smooth 1-D resistivity model derived from the integrated TM mode response of the entire GB-CP line was used as starting guess and a priori adherence section for our 2-D inversions (see Appendix A). It can be considered as an average host within which lateral heterogeneity lies, and is plotted next to each inversion section. Its starting model was a 100 ohm-m half-space down to 410 km depth, beyond which 5 ohm-m was imposed. The resulting smooth 1-D model down to 410 km is close to a half-space just under 100 ohm-m, except for the depth interval 4–12 km which has more resistive upper-middle crust of 200–300 ohm-m. Because the 2-D inversions work to keep models close to the a priori structure, first-order features in the final models should be significant. As a form of response sensitivity test for appraising models and verifying suspected 3-D effects, we compared 2-D models derived using various subsets of the full TM-TE-K_{zy} data.

3.3.2. Model Using TM Mode Data

[35] Numerous 3-D model studies have generally affirmed that 2-D inversion of the nominal TM (yx) mode data over a structure which terminates somewhere along strike yields cross-sections which recover object location reasonably well [*Wannamaker et al.*, 1980, 1984; *Jones*, 1983; *Wannamaker*, 1999; *Ledo*, 2005; *Siripunvaraporn et al.*, 2005]. Viability of TM models arises from inclusion of boundary charge effects from current flow along resistivity gradients in both 2-D and 3-D formulations. Even where the nearer-surface structure is rather arbitrary in shape, a well-sampled profile spanning the structural response still can provide good inversion models of deeper features because the mean effect of the shallower structure is compensated in the TM mode, allowing recovery of larger-scale resistivities and geometry [cf. *Torres-Verdin and Bostick*, 1992; *Wannamaker*, 1999]. A TM-only inversion is a prudent starting point for interpretation in light of the numerous rift grabens crossed, plus the NNE trends of the Phanerozoic sedimentary hingeline, Mesozoic overthrusting and deposition, Quaternary volcanism, and geomagnetic variation anomalies.

[36] The TM mode inversion model is shown in Figure 7 together with the computed responses of all data subsets. Several features appear which were anticipated from the observations. A low-resistivity (3–15 ohm-m) lower crust, mostly over the 15–35 km depth range stands out under the eastern GB and the TZ all the way to the major eastern physiographic scarp of the TZ at Thousand Lake Mountain. From analysis of the Pioche-Marysvale belt effect in Appendix A as introduced with the pseudosections, and as expected from diffusive EM fields, the lower crustal conductivity represented is presumably an average of potentially more detailed variation over a span of tens of kilometers north and south of the transect. There is a marked downwarp to ~50 km depth under the projection of the Wasatch Front (WF) corresponding to a near pinchout of the high φ_{yx} peak in that area,

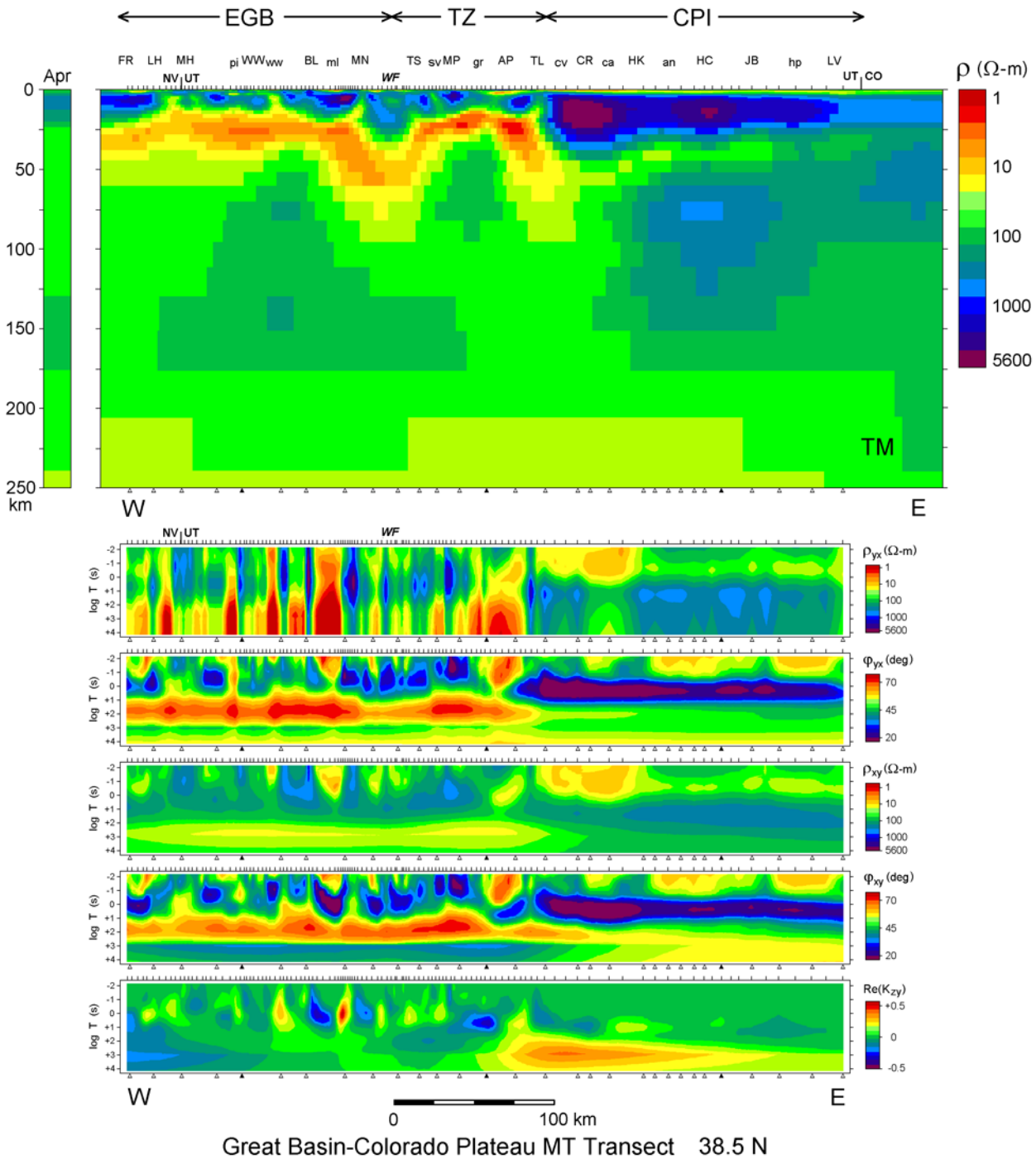

Figure 7. Two-dimensional inversion model of GB-CP transect considering TM mode data only. Computed TM and TE pseudosections are plotted below for comparison to data in Figure 5. Geographic locations and other labeling as in Figure 5.

and the layer dives and terminates at its easternmost end.

[37] Highly resistive middle and lower crust of the CP under Capitol Reef National Park abuts the GB-TZ conductor, which continues only weakly eastward in the 40–50 km depth range. Deeper CP resistivities in the 65–150 km depth range are greater (200–500 ohm-m) than those under the GB, but the GB values still are not low and reach 100 ohm-m over much of those depths. Beyond 200 km depth, GB and CP upper mantle resistivities appear similar for the TM mode although the

450 km aperture of our transect is reaching resolution limits there.

[38] The fit of TM mode computations to the observed in Figure 7 is very good; the latter are inevitably a bit rougher looking due to individual data point scatter and other small-scale complications. The graben finite strike effects on the observed TE impedance are clear as all computed sedimentary body TE responses are limited to T < 1 s. In particular, ρ_{xy} is quite smooth toward long periods and approaches a GB-wide minimum of ~20 ohm-m at ~1000 s corresponding to the lower crustal conductive layer. Below that, the TE calculations are close to 1-D over most of the GB segment, with ρ_{xy} rising to ~40 ohm-m by T = 10^4 s. This is classic 2-D TE mode response decay of a conductive stratum (lower crust) over resistive basement (upper mantle). In contrast, average observed ρ_{xy} across the eastern GB-TZ, analyzed more fully in Appendix A, rises to higher values, shows only a weak dip, and flattens to values near 80 ohm-m at the longest periods.

[39] Correspondingly, the computed φ_{xy} in Figure 7 shows a high in the period range 10–300 s over the GB-TZ due to the deep crustal conductor that is much stronger than in the observations and comparable to φ_{yx}. Model φ_{xy} also shows a minimum of <35° at 2000 s reflecting the rise in ρ_{xy} toward 10^4 s, well below the φ_{xy} data which barely fall to 45° under the Mineral Range area. The overall observed-computed TE discrepancy, we will show, is the combined effect of the Pioche-Marysvale belt inflating ρ_{xy} over middle periods, followed by a conductive upper mantle in the N-S direction flattening ρ_{xy} at the longest periods. Average GB ρ_{yx} (Figure A1) is just under 20 ohm-m by 10^4 s, less than the computed TE value. Thus there is an edge effect depressing ρ_{yx} and elevating φ_{yx} somewhat for T > ~2000 s over the GB area, presumably from termination of less resistive GB lower crust and upper mantle below Thousand Lake Mountain.

[40] The computed GB-side response in Re(K_{zy}) is small as observed, although there is a mild negative just west of the NV-UT border not in the data, presumably indicating the concentration of lower crustal conductivity in the Wah Wah-Mineral Range interval. Computed φ_{xy} on the CP side does not match the data for T > 100 s implying that the lower crustal conductor under the GB-TZ is insufficient to replicate it. The antisymmetric anomaly in Re(K_{zy}) at ~10 s under the Awapa Plateau is simulated but is weaker than the data. On the other hand, Re(K_{zy}) at long periods under the east edge of the TZ is well reproduced, reaching peak values of ~0.4 at 1000 s. This implies the MV anomalies measured by *Porath et al.* [1970] are due mainly to high conductivity in the lowermost crust. In detail, computed Re(K_{zy}) extends somewhat further east than observed toward 10^4 s.

[41] We added longer-period (T > 10 s) Re(K_{zy}) data with the TM responses in an inversion to incorporate the along-strike current flow of the TE mode. The tipper data are less prone to finite strike effects because these responses remain band-limited and do not suffer from "static" effects like the electric field [*Wannamaker et al.*, 1980, 1984; *Jones*, 1983; *Wannamaker*, 1999]. The resultant lower crustal conductor (not plotted) closely resembled that presented in the TM-only section, showing that bulk along-strike current flow supports a high-conductance lower crust under the GB extending through the TZ and ending abruptly in the Thousand Lake Mountain area. Computed Re(K_{zy}) at the longest periods under the eastern TZ was laterally more compact like the data, achieved by modest lower resistivity in the upper mantle toward the east end of the array near the Colorado border. However, fit to φ_{xy} for T > 1000 s under the eastern GB remained poor, in that observed values are much greater (~45°) compared to computations (~35°) as in Figure 7, and the high φ_{xy} under the CP is inadequately replicated. We demonstrate below with select inclusion of long-period φ_{xy} that low N-S upper mantle resistivity under the GB-TZ fits the overall response.

3.3.3. Select Inclusion of TE Mode Data

[42] Both finite strike extent of surficial sedimentary bodies and the resistive, E-W trending Pioche-Marysvale plutonic belt prevent straightforward inversion of the TE mode data. However, since the plutonic belt reaches a nearly static state in its ρ_{xy} and φ_{xy} response near 1000 s (Appendix A), φ_{xy} at longer periods primarily reflects upper mantle structure and can be utilized.

[43] Inspection of the data for T > 1000 s suggests that the GB-TZ upper mantle contains lower resistivity in the N-S direction than in the E-W. First, both TM mode and TM-K_{zy} data inversions plus inversions of Appendix A reveal similar quasi-horizontal, conductive lower crust under the GB-TZ area suggesting its estimated conductance is fairly robust. Having only a high-conductance layer near the Moho of the GB-TZ, with no plutonic belt effect, and resistive mantle below, ρ_{xy} should rise from a minimum like ρ_{yx} near 1000 s while φ_{xy}

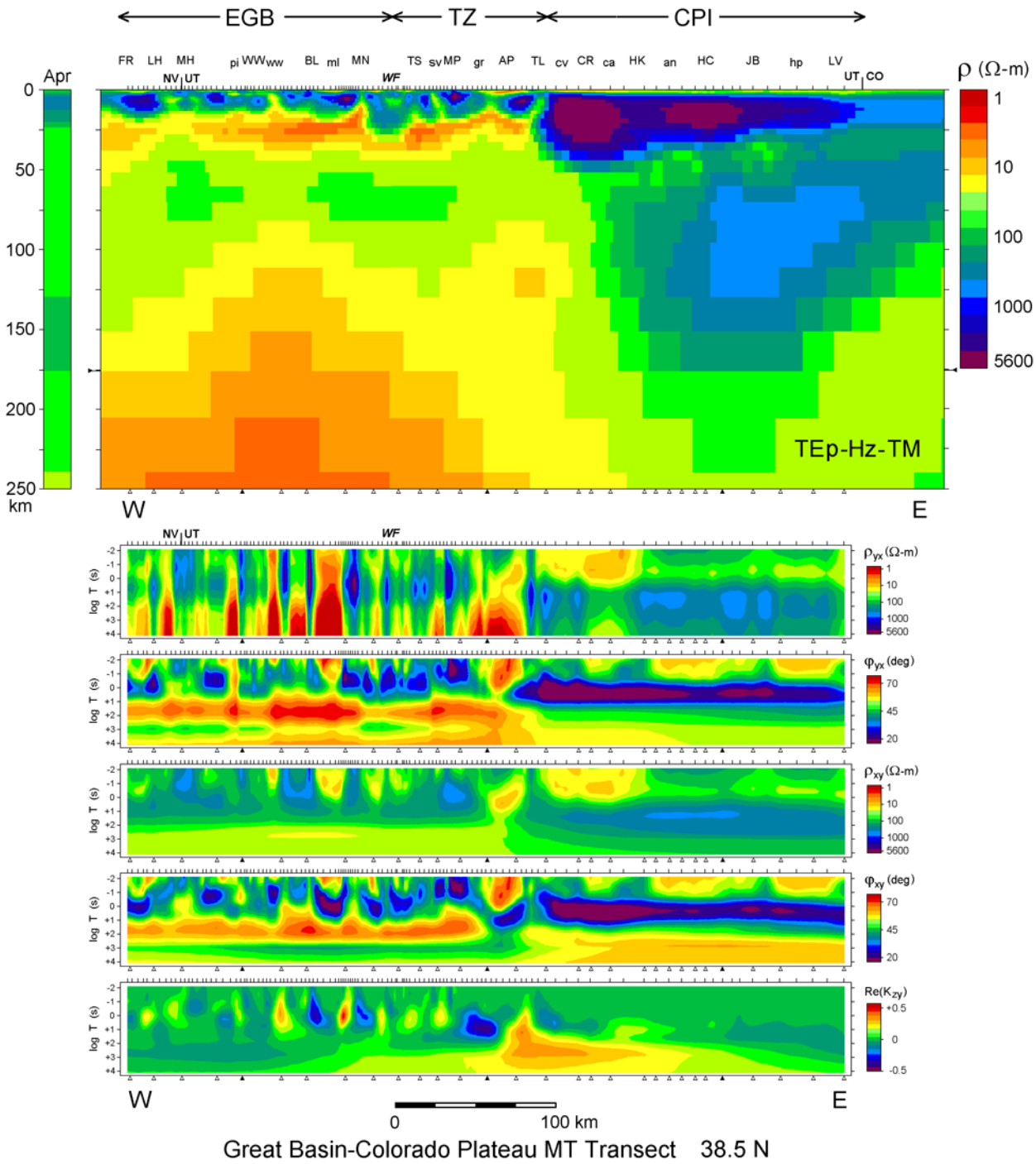

Figure 8. Two-dimensional inversion model of GB-CP transaction considering TM mode data for T < 50 s, real component of K_{zy} (tipper) data for T > 10 s, and TE mode phase for T > 1000 s. Computed TM and TE pseudosections are plotted below for comparison to data in Figure 5. Small arrows near 175 km depth along sides of model denote parameter boundary below which resistivities were fixed to the a priori values in the sensitivity test of Figure 9.

correspondingly falls to <35° near 3000 s (Figures 7 and A1). Moreover, though nearly static, the Pioche-Marysvale belt has a residual inflationary effect on the N-S electric field even for T > 1000 s, and so should swell ρ_{xy} and decrease φ_{xy} a bit more still. Hence, it is remarkable that the observed ρ_{xy} is nearly flat and $\varphi_{xy} \approx 45°$ for T > 1000 s. Adding in the depression of the E-W electric field and thus

ρ_{yx} by the abrupt east end of the GB-TZ lower crustal conductor, the near-parallel nature of the two ρ_a and φ data curves versus period in Figure A1 for T > 1000 s is coincidental and does not indicate upper mantle isotropy.

[44] Therefore, to get a rough image of N-S resistivity in the upper mantle, we invert GB-TZ φ_{xy} for T > 1000 s and CP φ_{xy} for T > 300 s, together with ρ_{yx} and φ_{yx} for T < 50 s, and Re(K_{zy}) for T > 10 s. Upper mantle structure dominates φ_{xy} at those long periods. The restricted periods of the included TM data constrain most of the crustal structure while preventing E-W resistivity of the upper mantle from having much influence. The K_{zy} data help resolve conductance of the lower crust, and show whether they have sensitivity to upper mantle structure.

[45] The resulting model and computed responses appear in Figure 8. Most notable in the section is the large region of low resistivity beneath the eastern GB especially below depths of ~100 km. Varying the period range of data inclusion somewhat has second-order effects on the absolute values of the low resistivity or on its breadth or depth to top, but the basic presence remains. In particular, increasing the period range of accepted TM data to 150 s serves to reduce slightly more the low resistivity of upper mantle below 100 km in the GB. Anisotropy factor is of order 3–10. It is difficult to estimate the shallow (<75 km) N-S mantle resistivity because its response overlaps further into the period domain of the plutonic belt (T < 1000 s); for this we need detailed 3-D surveying. The CP lithosphere takes on a simple resistive character, with a modest decrease in resistivity further east beyond and below the Colorado state border.

[46] The fit to the TM data appears good for T < 100 s, but computed φ_{yx} is significantly higher than observed for T > 1000 s. This shows that broadscale E-W resistivity in the upper mantle should not be low like the N-S. The fit of φ_{xy} for T > 1000 s is reasonably good over both GB and CP; the high over the CP at long periods we believe also is particularly diagnostic of low N-S upper mantle resistivity under the GB. Over the GB, computed φ_{xy} for T < 1000 s is higher than measured, while computed ρ_{xy} over most periods is lower than measured, reflecting the upward bias in the measured TE impedance by the Pioche-Marysvale belt. The fit to K_{zy} is slightly better than in Figure 7, although clearly the deeper upper mantle has weak influence upon K_{zy} in the measured period range. The anomalies measured by Porath and coworkers in Figure 4 are explained primarily by low resistivity near Moho levels in the deep crust of the eastern Great Basin and Transition Zone. Structure deeper than 200 km affects only very long periods of K_{zy}, 10^4 s and greater.

[47] Inversion test runs adding φ_{yx} for T > 1000 s were made to seek an isotropic model which fits both modes in regards to upper mantle resistivity, and reasonable fits to both φ_{xy} and φ_{yx} at long periods were possible (not plotted). The resultant deep structure showed two, narrow steep conductors under the GB-TZ separated by steep resistive zones including an amplification of the resistive deep lithosphere of the CP. This is classic clumping of resistivity media exhibited if fitting anisotropic data with isotropic models [*Heise and Pous*, 2001; *Wannamaker*, 2005]. The steep narrow conductors permit adequate north-south current flow to fit the TE observations, while the steep resistors prevent significant east-west current flow to fit the TM. Slight changes in data weighting during test inversions could radically alter the position of the steep conductors, or even lead to formation of three rather than two conductive concentrations, attesting to their instability and low physical significance. That is not to say such structures do not exist; the upper mantle mechanism causing the apparent anisotropy in Figure 8 could have a wide range of spatial scales from near-microscopic to tens of kilometers and have equivalent effect on MT responses. We view it as more conservative to present a model with broadscale anisotropy from separated MT data subsets.

[48] Finally, a test of depth extent of low, eastern GB resistivity structure in Figure 8 was made by forcing the inversion to place all structure at depths <175 km, with the a priori model preserved beneath. This inversion (not plotted) showed much lower resistivity than the unconstrained model (~1.5 versus 5–10 ohm-m) crammed into the narrow 150–175 km depth range under the eastern GB mainly between Pine Valley and the Tushar Range. Responses of the two models are compared in Figure 9 at the 1-year site in the Wah Wah Mountains, where we have the best data to the longest periods. The fit to φ_{xy} in the constrained inversion is only marginally worse than the unconstrained, so the two models may not be distinguishable based on φ_{xy}. However, the constrained model represents a less realistic, high-contrast alternative in our view. Thus, there still is a strong suggestion in the data of low resistivity in the N-S direction under the eastern Great Basin to depths of at least

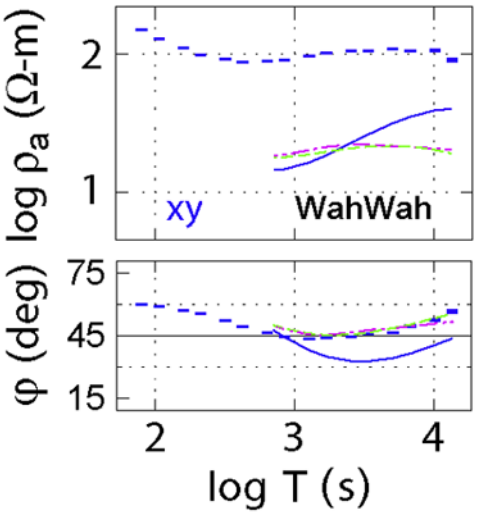

Figure 9. Observed long-period, nominal TE data at the 1-year occupation in the Wah Wah Range, compared with computations from the model of Figure 8 (green dashes) plus a test inversion of where all structure is constrained to lie in the upper ~175 km (pink dashes). Also plotted are the responses of the model of Figure 7, showing that high upper mantle resistivity as inferred with a TM inversion is incompatible with the TE phase (blue solid). Note strong upward static offset of observed ρ_{xy} compared to the 2-D models, argued in Appendix A to stem mainly from the Pioche-Marysvale belt under our transect.

200 km. Computations for the model of Figure 7 are shown in Figure 9 too, confirming that the TE data are incompatible with high upper mantle resistivities due to much lower φ_{xy} in the T > 1000 s range.

4. Physical State of the Great Basin–Colorado Plateau Transition From Resistivity Structure

[49] Numerous mechanisms can act in the crust and upper mantle to define electrical resistivity, so external constraints are needed to reduce nonuniqueness in the physico-chemical interpretation [*Wannamaker and Hohmann*, 1991; *Jones*, 1992, 1999; *Wannamaker*, 2000]. Even crude knowledge of deep temperature, composition and metamorphic grade, and geodynamic history may allow us to choose between competing mechanisms. The resulting improved picture of physical state in turn should enable refined geodynamic models for this enigmatic transition zone.

4.1. Pervasive Low Resistivity of the Deep Crust

[50] Low resistivity in the deep crust is inferred in many active extensional regimes [*Haak and Hutton*, 1986; *Wannamaker and Hohmann*, 1991; *Jiracek et al.*, 1995]. A first-order interpretation for the crust of the GB-TZ and the CP is given in Figure 10. Here, layered earth conductivity models as domain averages for the central GB and eastern GB-TZ are derived following *Wannamaker et al.* [1997a] by 1-D inversion of the TM mode integrated impedance from the respective MT profiles to periods of 1000 s. *Wannamaker et al.* [1997a] showed that the integrated MT responses were incompatible with a very thin deep crustal layer of equivalent conductance, but implied instead a distribution over depth. Added to the plot is the layered model similarly derived from the integrated CP curve of Figure A1 to 1000 s, which does appear thin. Finally, geotherms estimated from surface heat flow are plotted, including stretching in the GB areas [*Lachenbruch and Sass*, 1978; *Chapman et al.*, 1981; *Bodell and Chapman*, 1982]. Depth to top of conductive lower crust coincides with temperature of ~500°C in all three regions, affirming that the conductor lies in the ductile domain in active regimes and that its top is thermally controlled [*Hyndman et al.*, 1993].

[51] Even in the active eastern Great Basin where Moho level temperatures estimated from surface heat flow may reach 900°C [*Lachenbruch and Sass*, 1978], the electrical resistivity of dry silicate minerals is too high (~1000 ohm-m) to explain lower crustal values in the tens of ohm-m or less such as in Figure 10 [*Kariya and Shankland*, 1983]. This is a widespread phenomenon and low resistivity mineral boundary phases usually are invoked, primarily fluids or graphite [*Shankland and Ander*, 1983; *Hyndman et al.*, 1993]. In our study area, both late Proterozoic and Cenozoic igneous rocks imply deep crustal f(O_2) which was typically near the quartz-fayalite-magnetite (QFM) buffer, too high for graphite stability at current estimated temperatures [*Christiansen et al.*, 1986; *Carmichael*, 1991; *Van Schmus et al.*, 1993; *Parkinson and Arculus*, 1999; *John*, 2001], leaving us to prefer a fluid-based cause for low resistivity.

[52] A fluid must be compatible with composition and state variables (especially temperature) of the host rocks. The Proterozoic lower crust appears dominated by intermediate (Great Basin) to mafic (Colorado Plateau) metaigneous rocks ranging

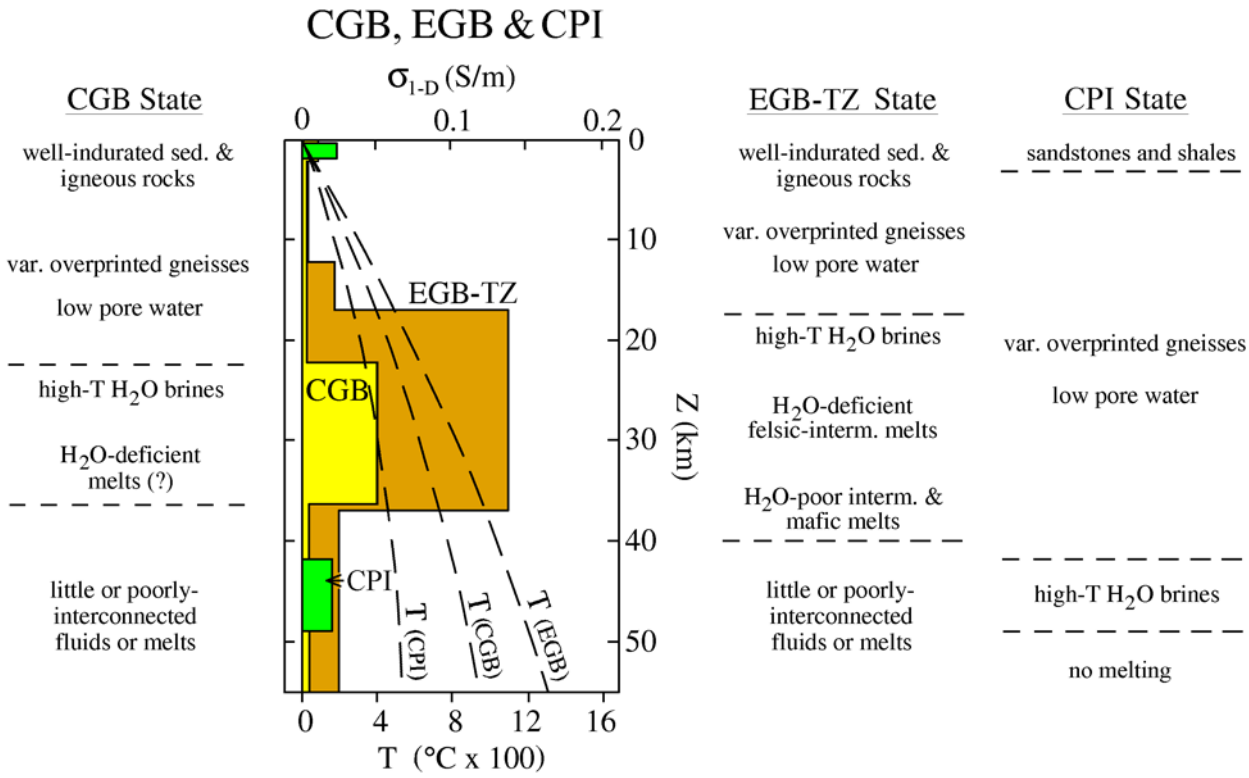

Figure 10. Layered earth conductivity profiles and their interpretation in terms of state of fluids/melting for central Great Basin (CGB), eastern Great Basin and Transition Zone (GB-TZ), and Colorado Plateau interior (CPI). Electrical properties are plotted as conductivity to emphasize differences in lower crust of the two regions, and because conductivity is more linearly proportional to content of conductive grain-boundary phases. These are 1-D inversions of TM mode response integrated along MT profiles for T < 1000 s, which is roughly equivalent to laying one long bipole the length of the profile and averaging out the effects of upper crustal heterogeneity within its span. Slightly modified from *Wannamaker et al.* [1997a] by incorporation of LIMS data to 1000 s, plus inversion of CPI data in Figure A1.

from deep crustal granulites to amphibolite, with greenschist facies at middle and higher levels [*Christiansen et al.*, 1986; *Van Schmus et al.*, 1993; *Wendlandt et al.*, 1993; *Nelson and Harris*, 2001; *Crowley et al.*, 2006], similar to deep continental crust elsewhere [*Rudnick and Fountain*, 1995]. In such high-grade metamorphic rocks, H_2O activity at 500–600°C must be $\ll 1$ so any fluid cannot be nearly pure water [e.g., *Yardley and Valley*, 1997]. However, complex multicomponent solutes can lower a(H_2O) markedly and appear sufficient to stabilize fluids at these conditions [*Aranovich and Newton*, 1997, 1998; *Wannamaker*, 2000]. Such fluids interconnect relatively well along mineral boundaries in the ductile regime [*Holness*, 1996, 1997], and are highly conductive [*Nesbitt*, 1993], requiring only small porosities (<0.5%) to achieve bulk resistivities <10 ohm-m with efficient pore geometries [*Grant and West*, 1965; *Wannamaker et al.*, 1997a].

[53] Conductivity mechanisms in the deeper, hotter portions of the GB conductive layers should differ from the upper portions [*Wannamaker et al.*, 1997a]. Toward the base of the GB conductors (near Moho), temperatures are high enough to permit H_2O-undersaturated melting [*Wannamaker*, 1986; *Clemens and Watkins*, 2001]. Hydrous silicic melts also interconnect well [*Laporte*, 1994], but are not as conductive as hypersaline fluids [*Wannamaker*, 1986; *Gaillard*, 2004] and thus require porosities of several volume percent to achieve $\rho < 10$ ohm-m [*Wannamaker et al.*, 1997a]. The integrated model for the CP points to only a weak conductive layer near the Moho [*Wolf and Cipar*, 1993] in keeping with a thin zone of high-temperature ionic fluids and no melting (Figure 10). A value of 500°C for layer top is toward the high end of the global range, but we view this as consistent with the dominant metaigneous lithology of the lower crust [*Wannamaker*, 2000].

[54] The pronounced lower crustal conductor of the GB and TZ should stem from underplated and crystallizing basaltic magmas near the base of the crust generated by recent and ongoing upper mantle melting events. These magmas exchange heat with the lower crust inducing partial melting, and release fluids upon crystallization. Several volume percent of H_2O-CO_2, highly saline brines typically are exsolved in this process [*Frost et al.*, 1989; *Wannamaker et al.*, 1997a], providing abundant conductive fluid. Under pure shear conditions without melting, lower crustal fluid release is unlikely because extension cools the crust as material rises in the solid state [*McKenzie*, 1978], resorbing fluids. *Wannamaker et al.* [1997a] showed that retention of the modest inferred fluid porosity obeyed fluid percolation models for ductile crustal rocks, provided there was ongoing fluid replenishment by basaltic underplating in the eastern Great Basin over the last 5–10 Ma. Mafic magma fractionation or remelting/hybridization is a leading hypothesis for production of distinctive topaz-bearing rhyolites which are common in the eastern Great Basin [*Christiansen et al.*, 2007].

[55] The 2-D deep crustal conductor (Figure 7) of course shows more complex attributes than a uniform layer. Depth to the top under most of the eastern GB and TZ is ~15 km as in the integrated model, but it deepens to near 25 km at the far western end toward the more quiescent central GB. The abrupt dip under the southern extension of the Wasatch Front may represent a particularly coherent and less extended package of Mineral Range-Tushar Mountains deep crust. We suggest that the depth to top of the deep conductor can be used as a proxy for the 500°C isotherm and represents a possible boundary condition for thermal modeling of the Transition Zone. This isotherm should closely parallel the brittle-ductile transition, argued by some to reflect a permeability boundary or change in mode of fluid interconnection [e.g., *Bailey*, 1990; *Hyndman et al.*, 1993; *Fournier*, 1999]. The lower boundary of the conductor, on the other hand, may be controlled more by compositional factors than thermal variations. It may be a natural basalt accumulation zone arising from melt-host rock buoyancy considerations, or it could reflect a decrease in fluid interconnection when passing from feldspar to olivine dominated lithologies [*Mibe et al.*, 1998]. The conductor is deepest just inside the CP from the TZ, implying a resistant lower crustal keel against the active terrane.

[56] A primary result of our study is the projection of conductive, thermally active and fluidized lower crust characteristic of the modern extensional eastern Great Basin eastward to the far end of the elevated Transition Zone at the Colorado Plateau interior. Given the slight degree of extension quantifiable at the TZ surface, it is clear that the vertically nonuniform rift scenario summarized in Figure 3b is more likely to represent TZ tectonism. Although a correlation with the rift pillow structure suggested from active and earthquake-source seismology is not guaranteed, the likelihood of significant basalt being underplated since end of Miocene time to supply the fluid is consistent with the seismic models. This would imply enhanced mantle upwelling and focused melting below the TZ, perhaps similar to recent models of volcanic continental margins [*Korenaga et al.*, 2002; *Gernigon et al.*, 2006]. Because termination of the lower crustal conductor against the CP appears to explain the geomagnetic anomalies of *Porath* [1971] in that area, it is intriguing to consider that their similar anomalies running N-S through central Colorado (Figure 4) have similar cause. That would be largely cryptic basaltic underplating of the crust from enhanced upper mantle melting [*Boyd and Sheehan*, 2005], despite little extension at the surface of the northern Rio Grande Rift.

4.2. Structures of the Brittle Crustal Regime

[57] Numerous dikelike conductors protrude toward the surface from the deep crustal conductor, especially in the vicinity of the TZ. An expanded view of this area is given in Figure 11, which also shows the model derived using the Rodi-Mackie inversion code demonstrating similarity of the main structures. Near the west end of Figure 11 is a west-dipping low-resistivity slab surfacing on the east side of the Mineral Mountains [*Nielson et al.*, 1986] just west of the Cove Fort geothermal resource area [*Ross and Moore*, 1985]. It connects to the locally intensified deep crustal conductor from there west to the Wah Wah Range. This is the same feature modeled and tested by *Wannamaker et al.* [1997b] in analysis of the wideband data from the Cove Fort area westward. It is interpreted to be a crustal-scale, fluidized fault zone connecting magmatic fluids of the lower crust with the meteoric regime closer to the surface [*Newell et al.*, 2005; *Crossey et al.*, 2006]. The conductor surfaces along the apparent feeder zone for a major Quaternary basalt flow extruded 300 ka [*Nelson and Tingey*, 1997] along the Cinder Knoll-Red Knoll

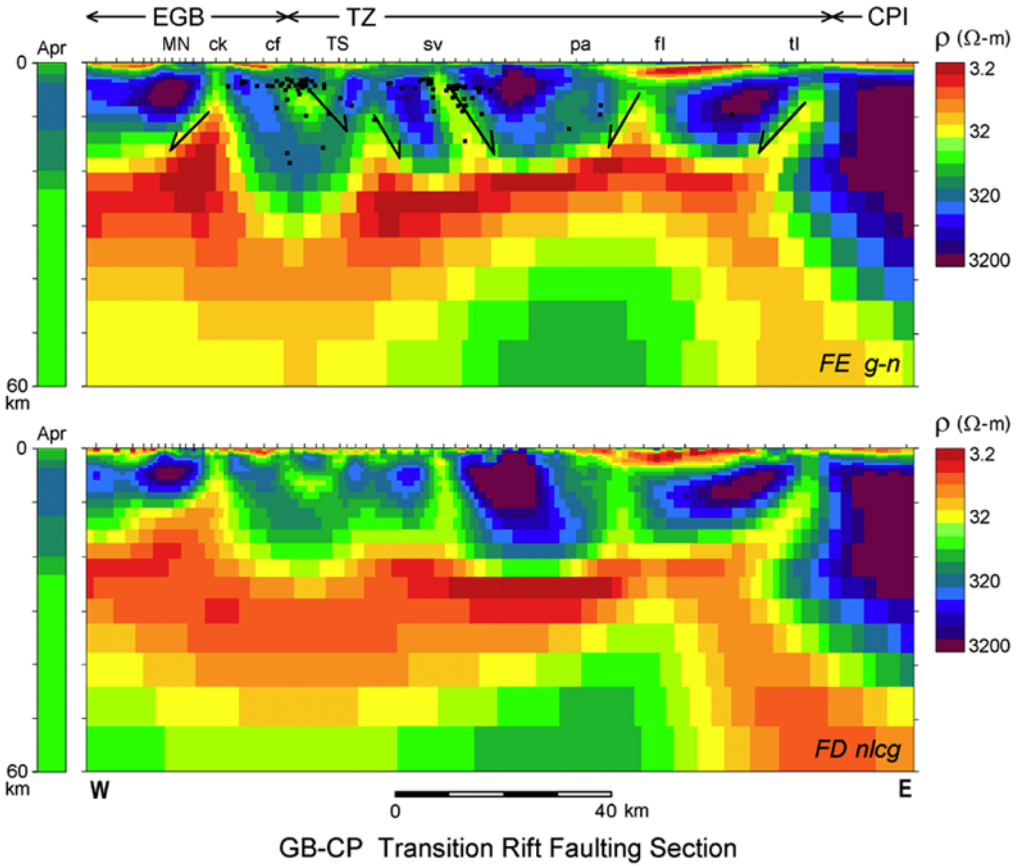

Figure 11. Focused view of resistivity structure of the Transition Zone highlighting steep conductive "fault zone" structure interpreted within and near Transition Zone. These zones probably are conductive due to fluids, but perhaps also somewhat to fluid-remobilized carbonaceous material (graphite). Landmarks include Mineral Range (MN), Cinder Knoll (ck), Cove Fort (cf), Tushar Mountains (TS), Sevier Valley (sv), Paunsagunt fault zone (pa) of Grass Valley, Fish Lake (fl) graben, and Thousand Lake Mountain (tl). This inversion is similar to Figure 8 except that we allowed TM mode data to 150 s to resolve uppermost mantle in this area. Also, we compare results from our 2-D inversion code (top) with that of *Rodi and Mackie* [2001] to demonstrate robustness of the main structures. Note color scale is adjusted slightly from Figure 8. Added to the top panel are the A and B quality earthquake epicenters of *Arabasz et al.* [2007] for a 25 km wide swath along our profile.

area. It may provide the elevated magmatic He^3 concentrations in the Cove Fort thermal waters [*Kennedy and van Soest*, 2006, 2007], although the precise shallow hydrology is obscure.

[58] The effect of such features on MT data is primarily in the TM mode, in particular causing abrupt lateral transitions in φ_{yx} even at longer periods (10–100 s). Such a step is visible in the TM pseudosections of Figure 5 and is reproduced well by the predicted model responses (Figure 7). The crustal-scale, steep conducting elements connect electrical currents induced in conductive upper crustal zones such as the grabens or older sedimentary sections, with the large-scale lower crustal conductor. They have shown up in numerous prior MT surveys [e.g., *Park et al.*, 1991; *Wannamaker et al.*, 1991, 2002], and a significant increase in misfit is generated if the conductive elements are deliberately disconnected in test inversion runs. *Wannamaker et al.* [1997b] plotted several soundings spanning the Cinder Knoll-Cove Fort conductor showing in detail the abrupt response behavior and the increased data misfit when broken. Perhaps a companion conductor is that which comes up under Wah Wah Valley, thus bounding a coherent segment of the upper crust from the Mineral Range through the San Francisco Range (Figure 7).

[59] Several high-angle conductive planes dip concentrically inward toward the central TZ and connect with the lower crustal conductive layer at that location (Figure 11). These features fit similar abrupt behavior in φ_{yx} at middle periods. Given

that incipient active extension is taking place in the TZ, we include interpretive normal faulting vectors with the presumed fluidized fault planes although the degree of slip is most likely small. The clearest plane in the TZ is that dipping steeply up to the west and connecting to the floor of N-S trending Sevier Valley. It is associated with the largest step in φ_{yx} in the central TZ, and in fact a narrow phase high is seen extending from middle to short periods under the valley. Along strike ~20 km to the north lies the Monroe-Joseph Hot Springs system [*Kilty et al.*, 1979], although we are not aware of sampling for He^3 there. Surface dip of the Sevier rangefront fault is westward [*Stokes*, 1986]; we suggest it may be antithetic to the crustal zone we have imaged. The steep conductor does not connect to recently described intense alunite alteration of the Whitehorse mine ~3 km to the east [*Rockwell et al.*, 2006], which generates a narrow band of low ρ_{yx} (Figure 5) but does not imply structure to depth. Another steep conductor appears to connect with the base of the Fish Lake graben, and the easternmost plane surfaces near the base of the eastern topographic scarp of the TZ just east of the Fremont/Thousand Lake fault zone [*Bailey et al.*, 2007; *Schelling et al.*, 2007].

[60] The nested geometry of the interpreted fault zones resembles synthetic normal detachments formed in continuum deformation models by *Nagel and Buck* [2004, 2007]. The modeling pertained to early stages of continental margin formation where rifting is symmetric but may be highly nonuniform vertically, with much greater extension in the uppermost mantle than in most of the crust [*Davis and Kuznir*, 2004; *Kuznir et al.*, 2005]. Such rifting occurs in a three-layer rheological geometry with relatively strong, brittle upper crust on a low-viscosity (weak) deeper crustal channel, all underlain by a stronger subdomain of mainly the upper mantle (the "jelly sandwich" strength model, reviewed by *Thatcher and Pollitz* [2008]). A correlation of stronger brittle crust with high resistivity is borne out by observed seismicity along our transect, which we have added to Figure 11. Where brittle upper crust overlies a deeply extending subdomain of low viscosity, normal faults instead tend to alternate in dip and strongly asymmetric deformation develops [*Nagel and Buck*, 2004, 2007]. As a zone of intense magmatic intrusion and hydrothermal fluid release, the deep crustal conductor of Figure 11 may represent the "jelly," consistent with possible enhanced mantle upwelling and fusion enabled by nonuniform extension versus depth. The domains of greatest fluid concentration will be those most prone to diffusion creep rheology in the dominantly feldspathic lithology, making for a very weak deep crust [*Tullis et al.*, 1996]. The uppermost mantle, and perhaps crystallized mafic underplate, would be stronger due to mafic/ultramafic mineralogy and its melt and H_2O depleted state.

[61] At the western end of the profile, the models of Figures 7 and 8 show two quasi-horizontal bodies of lower resistivity in the upper crust under the Wah Wah and Mountain Home Ranges. These are the regularized inversion equivalents of graphitized Paleozoic sediments interpreted to be underthrust beneath the Canyon Range and Pavant overthrust sheets of the Sevier orogenic era, as forward modeled by *Wannamaker et al.* [1997b]. They are distinct from the other upper crustal conductors in that they do not clearly connect to the regional low resistivity of the lower crust. In particular, the western package is resolved into two close pieces and separated by a prominent resistor between Mountain Home Range and Pine Valley from the Wah Wah conductor, as shown by *Wannamaker et al.* [1997b]. Possibly, a more finely discretized inversion emphasizing just the western district shorter-period data could simulate more of the details of the earlier forward modeling effort.

4.3. Physical State of the Upper Mantle From Resistivity

[62] Our interpretation of the state of the Great Basin–Colorado Plateau upper mantle from its resistivity including possible anisotropy is summarized in Figure 12, also incorporating the main crustal features just discussed. Upper mantle resistivities in the east-west direction under the eastern Great Basin in the 75–175 km depth range are of order 100 ohm-m (Figure 7). With oxidation state not far from QFM [*Christiansen et al.*, 1986; *Wood and Virgo*, 1989; *John*, 2001; *McCammon*, 2005], these are compatible with dry olivine-dominated mineralogy at T ≈ 1400°C [*Duba and Constable*, 1993; *Constable*, 2006]. A temperature of 1400°C is within the accepted global range of the average current mantle adiabat (ACMA, $T_p \approx 1350$°C), and argued to be the prevailing temperature profile for the GB and deeper CP on the basis of regional P- and S-wave tomography [*Goes and van der Lee*, 2002; *Kelley et al.*, 2006; *Herzberg et al.*, 2007]. Hence, despite the inference from presence of the lower crustal conductor of melt generated in the

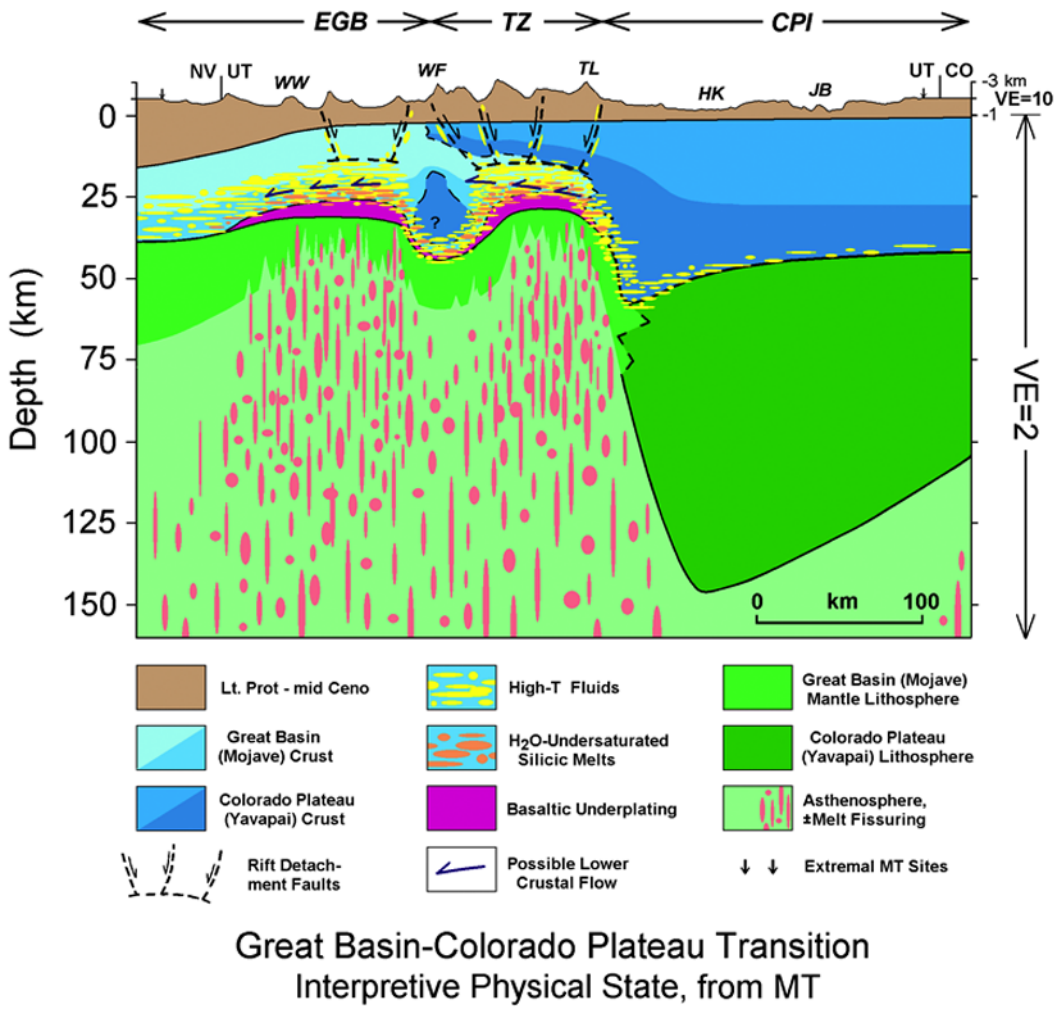

Figure 12. Schematic interpretation of physical state and terrane geometry across the Great Basin–Colorado Plateau transition emphasizing tectonics of the present day. A thick, competent CP lithosphere has persisted to the east since Precambrian time. Across an abrupt transition toward the Great Basin, concentrated mantle upwelling engenders fusion and melt focusing in N-S trending fissures toward the Moho. Basaltic melt ponding in lowermost crust induces crustal partial melting, exchange of heat, and exsolution of solute-rich magmatic fluids. Weakened lower crust may tend to flow westward to make space, and provide a boundary condition for nested detachment formation across the brittle upper half of the crust. Underlying the Tushar Mountains may be a remnant of Yavapai lower crust of an elongate N-S segment of Pioche-Marysvale plutonic rocks, locally impeding the flow process. Depending on style of interaction with deep east-moving asthenosphere, peridotite source may cycle through the melt zone plating residuum against CP keel, or upwell more symmetrically under the TZ.

upper mantle, there appears to be effectively no melt interconnection in the east-west direction.

[63] Inverting the nominal TE mode data required care because of the need to curtail finite strike effects, but we believe the data point firmly to lower N-S resistivity in the GB upper mantle even if precise depth and contrast are more elusive. The lower N-S resistivity suggests significant interconnected melt in that direction, consistent with north-south SKS fast trends in western Utah [*Sheehan et al.*, 1997; *Walker et al.*, 2004; cf. *Kendall*, 1994] and alignment of young volcanics fed by asthenospheric upwelling [*Nelson and Tingey*, 1997] (Figure 2e). Melt focusing planes are normal to directions of maximum extension [*Holtzman et al.*, 2003; *Spiegelman*, 2003], and with appropriate non-Newtonian rheology can be steeply oriented along strike of the rifting and focus toward a central axis [*Katz et al.*, 2006]. In Figure 12 we refer to this region as asthenosphere, realizing that it may be a region of both upwelled juvenile mantle and old lithosphere partially

melted. Additionally, steep melt sheeting may be induced by simple shear stresses on the margins of diapiric, partially melted upwellings [*Holtzman and Kohlstedt*, 2007], such as could be the case especially along the TZ-CP boundary.

[64] Alternate conduction mechanisms such as hydration of aligned olivine have been proposed to *Karato*, 1990; *Lizarralde et al.*, 1995; *Evans et al.*, 2005; *Wannamaker*, 2005]. However, recent lab data demonstrate that initial assumptions about hydrous solid state charge carriers are incorrect, and uncertainties exist about feasible measurement temperatures and grain boundary water effects [*Poe et al.*, 2005; *Yoshino et al.*, 2006, 2008; *Wang et al.*, 2006]; these issues make this mechanism a less likely explanation in our view. Therefore, since either north-south aligned olivine a axes or melt fissuring could induce north-south SKS fast directions [*Kendall*, 1994; *Vauchez et al.*, 2000; *Holtzman et al.*, 2003; *Katz et al.*, 2006], resistivity anisotropy may be reducing geophysical ambiguity and arguing for melt to at least contribute. TE mode MT responses tend to be broader laterally than TM, and increased east-west aperture to our transect would be especially useful in bounding the western margin of the deep anisotropy, as well as possible increases in deep conductivity to the far east associated with the northern Rio Grande Rift extension. To resolve north-south properties better in the upper 75 km or so under the eastern GB-TZ, 3-D MT coverage would be necessary.

[65] In more detail in Figures 7 and 8, the most pronounced stretches of low resistivity in the deep crust are under the easternmost Great Basin (Wah Wah to Mineral Ranges) and the TZ (Sevier Valley to Thousand Late Mountain). These appear directly underlain by relatively high upper mantle resistivity in the east-west direction, but low resistivity in the north-south directions in corresponding areas. The east-west high resistivity thus located suggests melt depletion of the upper mantle source regions to supply the underplating of the lower crust, leaving a more refractory and drained mantle state on the mineral grain scale. Presumably there are still aligned melt fissures in this volume preserving the low north-south resistivity. This is conjectural, and it would be worth extended MT profiling westward across the Great Basin to see if correlation between anisotropic upper mantle and relatively intense underplating is consistent.

[66] If T = 1400–1450°C in the 100–250 km depth interval based on the E-W resistivity values above is plausible, then the deeply extending, low N-S resistivity in the upper mantle of the GB and TZ probably represents a hydrous alkalic melt of lowered melting point [cf. *Bureau and Keppler*, 1999; *Asimow et al.*, 2004]. Less likely would be dry melt in a high-temperature upwelling (plume material) with T_p significantly greater than ACMA (1600°C at 200 km) [*White and McKenzie*, 1989]. Deep fluids and alkalis could derive from former oceanic crust of the foundered Farallon plate [*Humphreys et al.*, 2003; *Smith et al.*, 2004; *Usui et al.*, 2006] or be residual to Precambrian lithospheric formation [*Thompson et al.*, 1997; *Wannamaker et al.*, 2000].

[67] Estimates of effective melt fraction in the N-S direction of the upper mantle depend on interconnection geometry plus the temperature and composition of the melt phase. An end-member texture of steep melt sheets is highly efficient so that bulk conductivity is just the product of melt conductivity and porosity ignoring the solid state olivine [*Grant and West*, 1965]. At ~1400°C, an alkaline melt may be only ~0.04 ohm-m [*Roberts and Tyburczy*, 1999], and probably even less with dissolved water. Thus bulk resistivity of 5 ohm-m could result from porosity well under 1%. However, this is a minimal porosity based on adopting the smooth model of Figure 8 and assuming that porosity is not tortuous. We do not attempt to interpret porosity within the MELTS model framework [*Roberts and Tyburczy*, 1999; *Park*, 2004] due to uncertainty in abundance of alkali-rich and other incompatible components [*Wannamaker et al.*, 2000].

[68] A resistive Colorado Plateau upper mantle extends to depths of ~150 km and is a downward continuation of its tectonically inactive lithosphere from what was imaged for the crust. Values of 300–500 ohm-m in places are too high to reflect ACMA temperatures even in dry lithology, and so a relatively cool CP lithosphere is implied. Uppermost mantle earthquakes described by *Wong and Chapman* [1990], though rare, are no surprise in light of this. However, it is counter to some inferences that the CP lithosphere thickness is well under 100 km [e.g., *Lastowka et al.*, 2001] or that a mobile lower crust flowed eastward beneath the CP from the GB in middle to late Cenozoic time [*McQuarrie and Chase*, 2000]. The greatest thickness is adjacent to the TZ, again depicting a keel-like geometry as with the crust. The geometry is compatible also with the presence of rare lamproite magma emplaced during the early Miocene transi-

tion from calc-alkaline plutonism to Great Basin extension, magma that has been interpreted to originate in highly metasomatized upper mantle at such depths [*Wannamaker et al.*, 2000]. Unfortunately, it is difficult to constrain lithospheric depth extent toward the Colorado border at the edge of the MT data coverage.

4.4. Controls on the Locus of the GB-CP Transition Zone

[69] Although each major tectonic event along the TZ since Precambrian time will have conditioned it for future deformation, we view the ultimate control on Transition Zone activity as lying with the Mojave-Yavapai suturing which runs roughly along the same trend. The Mojave lithosphere despite being older than the Yavapai appears to have been rheologically weaker and accommodative for the Late Proterozoic rifting which defined western North America and the Cordilleran Hingeline [*Lee et al.*, 2001; *Nelson and Harris*, 2001]. This is attributed to the Mojave upper mantle retaining a greater state of melt fertility (less refractory) and its lower crust being more siliceous compared to the Yavapai. Subsequently, orogenic collapse with disappearance of the Farallon plate and formation of the San Andreas transtensional system concentrated Great Basin extension in former Mojave lithosphere up to, and at depth within, the GB-CP Transition Zone.

[70] The three occurrences of Precambrian basement rocks along the Transition Zone in Utah lie essentially at its western margin, the Wasatch Front [*Nelson et al.*, 2002]. Curiously, their isotopic compositions all are interpreted to reflect formation or cratonization ages of ~1700 Ma, which is close to that of the Yavapai province. While three is not a large sample number, we suggest that the upper portions of TZ basement may be mostly Yavapai while the lower may be more Mojave (Figure 12). The former terrane could have been placed northwestward over the latter in regional overthrusting during Proterozoic assembly, shortly after 1700 Ma [*Nelson et al.*, 2002]. Such a thrust vergence has been interpreted from field relations for suturing of Yavapai terrane to the Wyoming craton to the northeast [*Sims and Stein*, 2003]. The geometry may contribute to a cryptic mobilization of weaker lower crust beneath more competent upper crust in the TZ. Thus, we interpret strength variations as being the primary control on the nature of GB-CP transition deformation, with important modulating forces perhaps associated with early Pliocene Pacific Ocean plate reorganizations [cf. *Wernicke and Snow*, 1998; *Sonder and Jones*, 1999; *Hammond and Thatcher*, 2004; *Flesch et al.*, 2007].

[71] The intensity of the lower crustal conductor under the Transition Zone, plus the high heat flow and other thermal indicators, implies concentrated magmatic input not evident in the deformation immediately above. This points to nonuniform extension versus depth, bringing up the question of accommodation space for enhanced rifting. Since a master simple shear detachment at the surface [*Wernicke*, 1985] has remained difficult to identify, nonuniform deformation may be utilizing shear zones cryptic to the surface and lying subhorizontal deep in the crust. Flow of weakened lower crust of the TZ westward toward the GB may be one manifestation of this, similar to the lower crustal "occlusion" model of *Wernicke* [1992]. The deeper root of the western Tushar Mountains may require some out-of-plane flow component. Concentrated magmatism below the TZ could signify mantle buoyancy and dynamic upwelling to help elevate the Transition Zone.

4.5. Comparison With Southern Sierra Nevada and Western Great Basin

[72] Vertically nonuniform extension largely cryptic to the surface also has been interpreted under and immediately east of the southern Sierra Nevada of eastern California [*Wernicke et al.*, 1996; *Jones et al.*, 2004]. Lower crustal flow eastward to the California Basin and Range plus buoyant upper mantle support of the elevated Sierra are inferred on the basis of a nearly flat seismic Moho depth and from low upper mantle seismic velocities and low electrical resistivities [*Jones et al.*, 1994; *Park et al.*, 1996], perhaps exploiting ancestral compressional fabrics [*Jones and Phinney*, 1998]. Destruction or delamination of prior upper mantle in the Pliocene coincident with potassic mafic magmatism, westward encroachment of extension, and Sierran uplift mark establishment of the buoyancy, representing probable partial melt and depletion of dense garnet [*Ducea and Saleeby*, 1998; *Farmer et al.*, 2002; *Jones et al.*, 2004]. Possible remnants of old lithosphere under the west margin of the Sierra have been imaged teleseismically and with MT [*Zandt*, 2003; *Park*, 2004]. The Sierran situation resembles that of the GB-CP transition in exhibiting distinctly later activity relative to Great Basin

proper (earliest Pliocene in our case) including uplift and a migrated phase of younger rifting, replacement or destruction of mantle lithosphere through upwelling and melting, a resistive lithosphere inboard of the extensional zone, and possible lower crustal flow toward the previously extended domain perhaps exploiting early fabric (Yavapai-Mojave suture for us).

[73] Several subvertical, crustal-scale conductors connecting to conductive lower crust also were imaged in the California Basin and Range by *Park and Wernicke* [2003], and interpreted to be major strike-slip fault zones. Strike slip motion is not implied in the zones we have imaged in Figure 11, just probable fluid egress from deep crustal magma degassing and possible mixing with meteoric waters. Three major, steep conductive fault zones connecting to inferred active basaltic magma underplating also were imaged in a 350 km long, wideband MT transect across the northwestern Great Basin by *Wannamaker et al.* [2006a, 2006b]. The central of these connects with the Dixie Valley high-temperature geothermal system, which exhibits an anomaly in mantle He^3 indicative of recent magmatic input [*Kennedy and van Soest*, 2006, 2007]. Situated in the Central Nevada Seismic Belt [*Niemi et al.*, 2004; *Hammond and Thatcher*, 2005], this steep trend is taken to represent a fundamental fluidized damage zone from repeated earthquakes including several historic events of M > 7 [*Niemi et al.*, 2004; *Hammond and Thatcher*, 2005; *Hammond*, 2005]. A second under central Nevada subcrops at the newly recognized McGinniss Hills geothermal area [*Coolbaugh et al.*, 2005a, 2005b] while the third to the west is not yet identifiable at the surface. That conductor, with its pronounced westward dip, may exploit earlier Mesozoic thrust fabric [*Wyld*, 2002].

5. Conclusions

[74] Wide-aperture, well-sampled, broadband MT data sets have a unique potential to provide views of extensional geodynamic processes over many length scales, from 100 km in upper mantle melt source regions to 10 km at Moho levels where basaltic melts are ponded, emit fluids and reduce crustal viscosity, to 1 km where the upper half of the crust is taken apart during rifting. In the Great Basin–Colorado Plateau transition in Utah, weak extension at the surface masks intensive magmatic underplating and fluid exsolution in the lower crust, every bit as pronounced as the more obviously active eastern GB. However, surface indications imply that onset of activity in the Transition Zone is later than the Great Basin proper, occurring mainly since end of the Miocene. Crustal-scale faulting patterns in the TZ are reminiscent of nested detachments modeled to form in the "jelly sandwich" model of crustal rheology, where the magmatically fluidized lower crust is the weak layer. In concert with other studies in the Great Basin, steep crustal-scale faults connect a deep, dominantly magmatic fluid regime with the meteoric zone of the upper crust.

[75] The termination of high-conductance lower crust against the competent CP lithosphere appears sufficient to explain the anomalies in magneto-variational data of Porath, Gough, and coworkers, thus resolving a long-standing ambiguity as to whether their anomalies had a Moho-level or a deep upper mantle origin. The upper mantle below the Great Basin probably has an effective anisotropy with the N-S direction being up to 10 times more conductive than the E-W. With likely ACMA temperatures, the physical model depicted is one of depleted, melt-disconnected peridotite in its E-W fabric, but with steep melt fissuring directed N-S. Additional transect coverage of the GB westward is advocated to confirm that, but it is in keeping with shear wave splitting directions and extensional melting models. The boundary to the CP on the east side of the transition is abrupt, with a resistant CP keel manifest in both the deep crust and mantle lithosphere to ~150 km depth. This likely represents the edge of a suture zone dating to the middle Proterozoic which has determined the shape of tectonism since. Strength variations control the style of deformation across the transition, modulated by various possible forces from the plate boundary, gravitational potential energy, basal traction and dynamic mantle upwelling. Specifically, a crustal-scale overthrust geometry of harder Yavapai rocks over weaker, tectonized Mojave rocks may contribute to the cryptic nature of activity under the Transition Zone. Nevertheless, along-strike changes in lower crustal strength exist under the TZ as evident in the persistence of the Pioche-Marysvale belt effect there.

[76] Large MT data sets over repeatedly deformed terrains also present a challenge for implementing resistivity models of appropriate dimensionality (2-D versus 3-D) and material properties (isotropic versus anisotropic). The evident finite strike effects of the conductive Great Basin alluvial grabens are just one factor tempering use of the TE mode in 2-D

modeling, and even a small amount of offline MT data was valuable in establishing a structural framework within which to optimize 2-D modeling. We believe it has been safer to start with inversion of nominal TM mode data to build a sectional resistivity model, as this accommodates abrupt response behavior when crossing resistivity boundaries and recovers larger scale averages of resistivity well when spanning the anomalies. Broad-scale comparisons between the modes, in light of known or probable changes in lithospheric architecture and tectonic activity, can help one to bracket 3-D influences and reveal the most robust structures. Nevertheless, 3-D data coverage and modeling ultimately will be needed to improve resolution and reduce ambiguity of certain elements.

Appendix A: Effect of the Pioche-Marysvale Plutonic Belt

[77] Justifying the basis for using a 2-D interpretation approach is a major component of MT transect studies. We place the analysis of an apparent important cross-line structure in this appendix to preserve flow of the main text regarding final cross sections and their tectonic inferences.

A1. Regional Integrated Impedance Soundings

[78] Broadscale averages of the impedance response can provide insight to the influence of structures with scales comparable to transect length and guide the modeling approach. To distinguish average characteristics of the GB-TZ and CP responses, we plot in Figure A1 the integrated impedance soundings derived from the ensembles of sites to the west and to the east of Thousand Lake Mountain, where the lower crustal GB-TZ conductor appears to terminate. For the TM mode, such an integration of the impedance yields a single response curve equivalent to an E-field bipole the entire width of the integration (~200 km each in this case) [*Torres-Verdin and Bostick*, 1992; *Wannamaker et al.*, 1997a]. This effectively suppresses the influence of crustal structures with characteristic width less than that of the integration. Such suppression of heterogeneity is not guaranteed theoretically for the TE mode, but its integrated responses will be revealing also.

[79] The eastern GB-TZ integrated responses in Figure A1 show two main features. First, ρ_{yx} and ρ_{xy} are nearly isotropic from the short periods to ~1 s; no static shift adjustment was made to either curve. The short-period value ~80 ohm-m is similar to that derived for the central GB of northeastern Nevada [*Wannamaker et al.*, 1997a], and appears characteristic of the upper ~5 km of the miogeoclinal Phanerozoic sedimentary section of the Great Basin with intermixed Cenozoic intrusives. Second, beyond ~1 s we have $\rho_{xy} > \rho_{yx}$ increasingly, to a factor of ~4.5 for T > 1000 s. In relation, φ_{xy} falls below φ_{yx} for $1 < T < 1000$ s before returning to values close to φ_{yx} for T > 1000 s. The behavior was pointed out with the ensemble of soundings over the GB-TZ span in Figure 5 and appears to extend westward at least to the Nevada border.

[80] In section A2, we show from long-period MT stations off-transect that this ρ_a and φ divergence likely results from the relatively resistive, narrow E-W Pioche-Marysvale plutonic belt underlying our profile (Figures 2d and A2). Thereby the N-S electric field becomes inflated toward longer periods causing the two ρ_a curves to split, reaching a nearly static limit by ~1000 s. We further argue that its effect on the TM response should be minimal. This allows a 2-D inversion emphasizing the TM mode together with long-period TE phase and vertical H-field, as elaborated in the main text.

[81] The integrated responses of the CP sites also are isotropic in the upper period range (Figure A1). Absent is the pronounced divergence of ρ_{xy} over ρ_{yx} toward T > 1000 s seen in the GB data; its lack commences in the MT stations almost immediately east of Thousand Lake Mountain (Figure 5), confirming that the GB-TZ broad anisotropy is caused by a narrow E-W structure there. A slight drop in ρ_{yx} and peak in φ_{yx} near T = 100 s on the CP curves suggest a weak conductor near its Moho. We do not see such in ρ_{xy} and φ_{xy}, but modeling in the main text showed that its TE response merges with the larger mode divergence beyond 300 s. As noted with Figure 5, inversions will imply that this large anomaly primarily reflects influence of the conductive lower crust of the GB and TZ laterally, and of more conductive GB-TZ upper mantle in the N-S direction.

A2. East-West Trending Pioche-Marysvale Belt and Two-Dimensional MT Interpretation

[82] A systematic inflation of ρ_{xy} relative to ρ_{yx} for T in the 1–1000 s period range, accompanied by $\varphi_{xy} < \varphi_{yx}$ over similar periods, is characteristic of the entire GB-TZ profile segment, but not the CP segment (Figure A1). To identify the cause of the

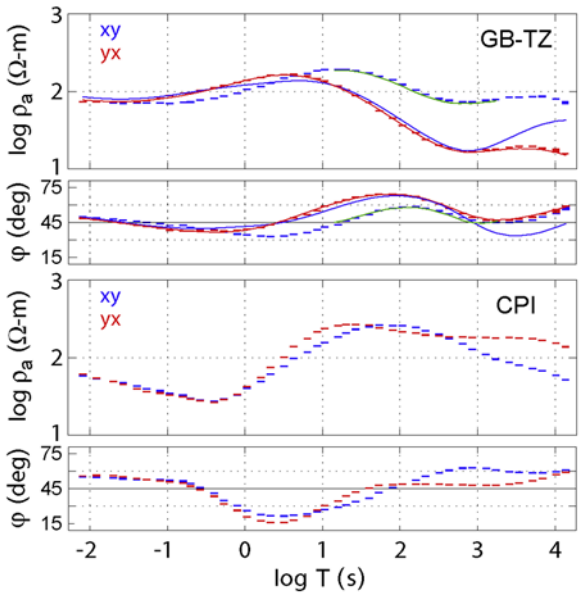

Figure A1. Integrated impedance sounding curves from the data of Figure 5 over the two distinct tectonic divisions of the study area, the Great Basin–Transition Zone (top) and the Colorado Plateau interior (bottom) divided at Thousand Lake Mountain. Error bar heights are two standard deviations. Computed curves in the GB-TZ panel are the integrated TM (red) and TE (blue) responses of the TM mode inversion of Figure 7. Similarly good fits to the TM data were obtained in the TM inversions of Figure A2. Computed ρ_{xy} fitting the inflated integrated ρ_{xy} (green) is from 2-D inversion of the xy data across sites MS-WW-BC over the Pioche Marysvale belt (Figure A2).

effect and a way forward for 2-D inversion, four long-period MT stations were taken off-transect in the eastern GB. Two are ~50 km to the north in the Barn Hills and northern Cricket Range, and two are ~50 km to the south off the Wah Wah Range (Mountain Spring) and in Long Hollow (Figure 1). With the data of the main transect, these constitute two, three-station profiles ~100 km long running N-S separated by ~50 km east-west. The southerly sites lie south of the Blue Ribbon transverse zone and the northerly ones lie north of the Cove Fort zone [*Rowley et al.*, 1998].

[83] Site pseudosections of impedance phases and $Re(K_{zx})$ for these sites appear in Figure A2. Apparent resistivities are not plotted because substantial site-site static offsets obscure the pertinent relative variations between stations, but we will introduce ρ_a to the inversion via the integrated impedance. For $Re(K_{zx})$, values of the main line are those at the yearlong site in the central Wah Wah Range (WW, west) and the LIMS site on the west side of the Mineral Range (MN, east). For φ_{xy} and φ_{yx}, values of the main line are those of the integrated impedance curves of Figure A1 in order to avoid residual local site complications in the impedance.

[84] In viewing these results, we essentially have turned the mode identification sideways from that of the main transect. Because they pertain to the E-field directed E-W along the Pioche-Marysvale belt, ρ_{yx} and φ_{yx} are analyzed as TE mode while ρ_{xy} and φ_{xy} are analyzed as TM. This is viable because we are considering band-limited quantities not prone to substantial static effects over the finite frequency range of the Pioche-Marysvale belt. For both profiles, φ_{yx} shows a smooth transition from lesser peak values in the south to higher peak values in the north in the 20–300 s period range. This is suggestive of a straightforward gradient in the conductance of the lower crustal conductor over this distance as far as the TM mode data are concerned.

[85] However, the integrated impedance φ_{xy} shows a distinct pinchout at the central sites of each profile (WW, MN). This corresponds to the inflation of ρ_{xy} over the 1–1000 s period range described previously with the main transect, a relative inflation not occurring in the ρ_{xy} curves of the southern (LH, MS) or northern (CR, BC) stations (not plotted). It suggests a local, E-W trending crustal resistor under the central sites boosting the N-S electric fields, as suspected. The anomalous behavior of φ_{xy} at the northern sites is quite strong, denoting an E-field dropping to such small values that minor 3D or anisotropic structure may be imposing some instability there [cf. *Wannamaker*, 1999, 2005]. Nevertheless, these sites obviously lie on the conductive side of an E-W boundary. The longer-period negative anomaly in $Re(K_{zx})$ under the western end of the transect (Figure 5) appears, on the basis of the western three-site profile, to be local to the transect.

[86] Figure A2 shows 2-D inversions of the short profiles using the same a priori model as for the main transect. To provide apparent resistivity control, the integrated ρ_{xy} and ρ_{yx} of Figure A1 were applied to the central sites MN and WW. Our purposes in the inversion are narrow and we do not promote many model details. We wish simply to establish a cause for the broadscale anisotropy which we believe lies in the crust, and evaluate its basic ramifications for TM mode inversion of the main transect and for inclusion of select portions of the transect TE responses. Included periods are

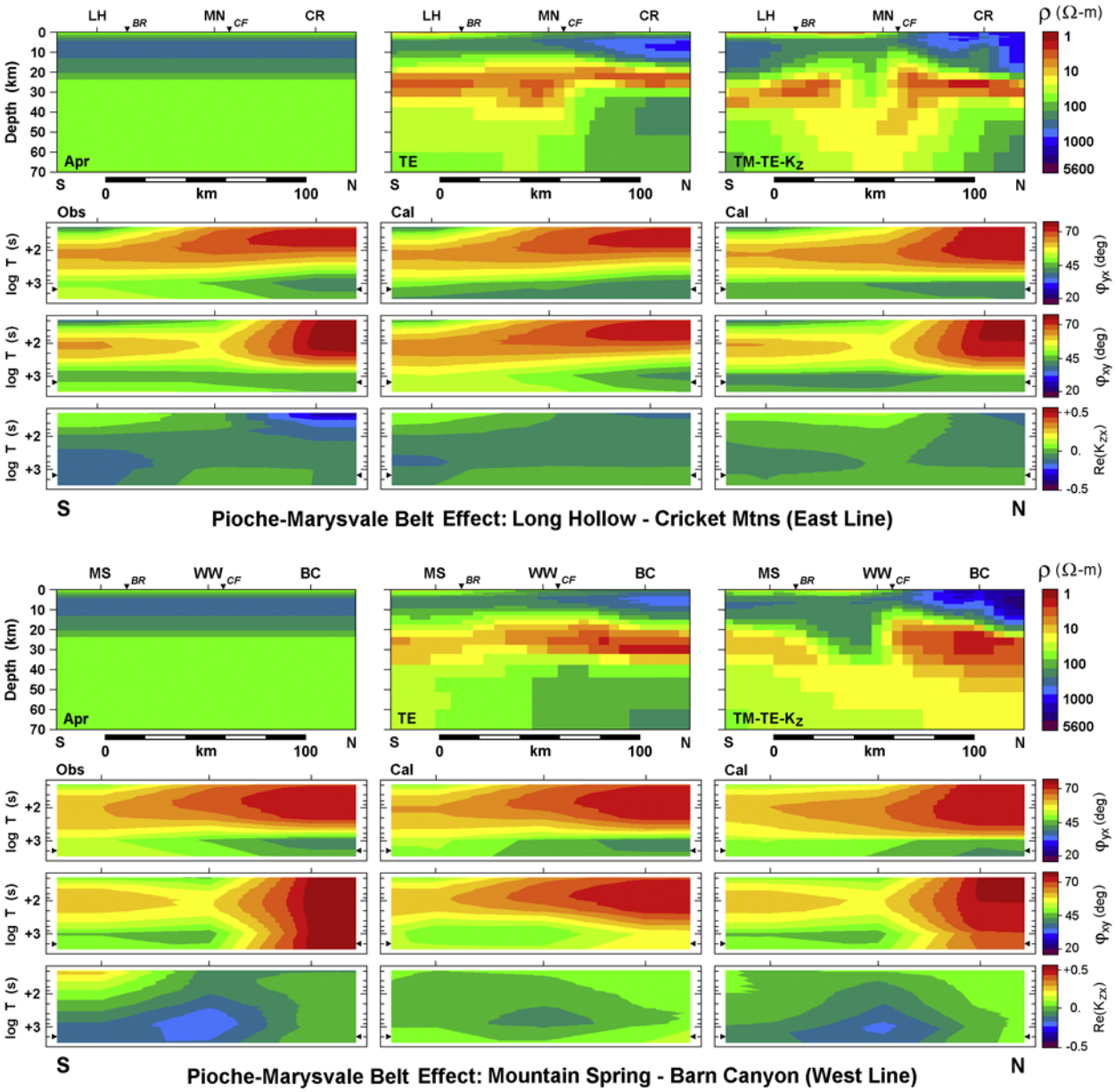

Figure A2. Observed and modeled impedance phase and vertical H-field responses for two three-site profiles running N-S across our main MT transect of Figure 1. North remains the *x* axis while *y* is east. The top set of panels pertains to the eastern short profile, while the bottom set pertains to the western profile. Model panels from left to right are a priori and starting 1-D section, TE only inversion of ρ_{yx} and φ_{yx}, and joint inversion emphasizing the TM mode responses (φ_{xy}, downweighted ρ_{yx}, φ_{yx}, and Re(K_{zx})). Black arrow heads denote long-period limit of data allowed into inversion for each profile. Sites are labeled Long Hollow (LH), Mineral Range (MN), Cricket Range (CR), Mountain Spring (MS), Wah Wah Mountains (WW), and Barn Canyon (BC). The Blue Ribbon and Cove Fort transverse zones are BR and CF.

<1500 s for the eastern profile and <2000 s for the western to ensure minimal sideswipe by the transition to the Colorado Plateau under Thousand Lake Mountain, although we show calculations to 3000 s to illustrate overall response of the crustal structures. We do not plot models to depths much beyond the Moho because profile aperture is only ~100 km.

[87] Inversions of φ_{yx} only (TE mode in this orientation) with integrated ρ_{yx} control show that the Pioche-Marysvale belt probably does not seri-

ously bias the TM inversions of the main profile (Figure A2). Good fits were obtained to the phases and to integrated ρ_{yx} at MN and WW, which fell to ~18 ohm-m at T = 2000 s (Figure A1). The sections show a laterally smooth lower crustal conductor with similar conductance across south to north, or perhaps somewhat more conductive to the north under the more-extended Sevier Desert. Conductances are similar to those across the GB-TZ in the TM mode transect inversion of Figure 7. In part, the higher phase φ_{yx} in the north is simulated by creating high contrast between upper and lower crust, rather than a mere decrease in deep resistivity from the a priori 1-D values. Further resolution would benefit from parallel MT station profiling to the north across the amagmatic lithology to constrain its crustal resistivity section. Long-period K_{zx} is subdued across the eastern three-site profile in agreement with a quasi 1-D lower crust. The compact anomaly in K_{zx} under the Wah Wah site is not simulated in this inversion, indicating a local abrupt boundary that does not obviously influence the yx data response.

[88] TM mode inversion of ρ_{xy} and φ_{xy} in Figure A2 reveals a compact crustal scale resistor under each line below and slightly south of the central sites MN and WW. We allowed ρ_{yx}, φ_{yx} and $Re(K_{zx})$ data downweighted by a factor of four relative to TM to improve resolution utilizing E-W current flow. The pinchout in φ_{xy} under the central sites is reproduced well and ρ_{xy} reaches ~80 ohm-m near 1000 s (Figure A1). This is in contrast to computed ρ_{xy} from the transect TM inversion of Figure 7, which dips below 20 ohm-m like the TM before sensing resistive upper mantle (Figure A1). Anomalous phase due to the resistor appears to fall below 2–3° relative to surroundings, representing its near-static limit. The fit of $Re(K_{zx})$ under site WW of the western line is much improved by formation of the sharp lateral transition of the inversion model to high conductivity under Barn Canyon. The fit to ρ_{yx} and φ_{yx} is qualitatively good and could be improved by upweighting its influence; such models show even tighter lateral bounds on the resolved crustal resistor although the fit to ρ_{xy} and φ_{xy} is degraded somewhat. This suggests to us that subsidiary E-W shears to the Cove Fort and Blue Ribbon lineaments may exist within the Pioche-Marysvale plutonics to further diminish its effect upon ρ_{yx} and φ_{yx} but still allow high ρ_{xy}. These are rife in geological mapping of the region [e.g., *Nielson et al.*, 1986] and the transverse zones themselves have widths up to 25 km [*Rowley*, 1998]. Low computed $Re(K_{zx})$ is achieved for the eastern model by keeping lower crustal conductance nearly equal under the flanking sites LH and CR.

[89] To conclude, the broad anisotropy in ρ_a across the GB and TZ developing over the 1–1000 s period range can be explained by an E-W, crustal-scale strip of high resistivity only a few tens of kilometers wide. On geological grounds, we correlate it with the plutonic Pioche-Marysvale belt bounded on the north and south by the Cove Fort and Blue Ribbon transverse zones. Its narrow N-S extent explains the lack of similar anisotropy in the CP. The resistive Pioche-Marysvale belt locally disrupts the N-S electric field over the GB and TZ segment preventing straightforward joint inversion of the TM and TE responses. However, overall N-S current flow is not strongly affected as implied by the TM-K_{zy} inversion discussed in the main text. Because its effect is band-limited primarily to T < 1000 s, longer-period φ_{xy} should be dominated by upper mantle structure and thus can be used to help resolve N-S directed resistivity there in inversion of the main transect. The narrow resistor appears to have a very limited effect on ρ_{yx} and φ_{yx}, or may effectively be less resistive E-W due to subsidiary shearing. Thus 2-D TM inversion of the main profile should yield a reasonably accurate cross section provided one accepts that the deep crustal properties will be a N-S average over a swath of several tens of kilometer width.

Acknowledgments

[90] The data collection of this transect has taken place over nearly three decades, initially with support of the U.S. Department of Energy, Geothermal Program, under contract DE-AC07-79ET27002. Contract DE-AC07-90ID12929 and NSF grant EAR96-16450 also supported development of the University of Utah MT system which collected many of the wideband sites. Electronics engineers Dale Green and Steven Olsen are thanked for their essential contributions to system construction. Most of the field work was financed under NSF/Geophysics grants EAR81-16602, 84-17765, and 02-30027, plus State of Utah Mineral Lease funds. Quantec personnel John Donohue, Chris Early, Bruce Frantti, and Keith Morrison ensured high-quality wideband field collection, and Ken Nurse implemented the Parkfield remote referencing. The long-period LIMS instruments were borrowed from the University of Washington (John Booker, P.I.) through the NSF-supported EMSOC national MT pool. DOE contract DE-FG07-00ID13891 supported Wannamaker for development of the Utah 2-D inversion code applied to the data. Thanks go to Walter Arabasz and Kris Pankow for advice on central Utah seismicity. Personnel of Fishlake National Forest, Capitol Reef National Park, Canyonlands National Park, and Glen Canyon National Recreational Area kindly permitted site access and

clearances. Doug Jensen produced or finalized many of the illustrations. We thank Rob Evans and an anonymous referee and associate editor for valuable reviews of the initial submission. This paper is dedicated to the memories of Stanley H. Ward and Gerald W. Hohmann, Professors of Geophysics, who founded electrical methods research at the University of Utah and advanced it over many years.

References

Allmendinger, R. W. (1992), Fold and thrust tectonics of the western United States exclusive of the accreted terranes, in *The Geology of North America*, vol. G-3, *The Cordilleran Orogen: Coterminous U.S.*, edited by B. C. Burchfiel, P. W. Lipman, and M. L. Zoback, pp. 583–607, Geol. Soc. of Am., Boulder, Colo.

Arabasz, W. J., R. Burlacu, and K. L. Pankow (2007), An overview of historical and contemporary seismicity in central Utah, in *Central Utah—Diverse Geology of a Dynamic Landscape*, edited by G. C. Willis et al., *Utah Geol. Assoc. Publ. 36*, pp. 237–254, Salt Lake City.

Aranovich, L. Y., and R. C. Newton (1997), H_2O activity in concentrated KCl and KCl-NaCl solutions at high temperatures and pressures measured by the brucite-periclase equilibrium, *Contrib. Mineral. Petrol.*, *127*, 261–271, doi:10.1007/s004100050279.

Aranovich, L. Y., and R. C. Newton (1998), Reversed determination of the reaction: Phlogopite + quartz = enstatite + potassium feldspar + H_2O in the ranges 750–875°C and 2–12 kbar at low H_2O activity with concentrated KCl solutions, *Am. Mineral.*, *83*, 193–204.

Armstrong, R. L. (1968), Sevier orogenic belt in Nevada and Utah, *Geol. Soc. Am. Bull.*, *79*, 429–458, doi:10.1130/0016-7606(1968)79[429:SOBINA]2.0.CO;2.

Armstrong, R. L. (1982), Cordilleran metamorphic core complexes, *Annu. Rev. Earth Planet. Sci.*, *10*, 129–154, doi:10.1146/annurev.ea.10.050182.001021.

Armstrong, R. L., and P. Ward (1991), Evolving geographic patterns of Cenozoic magmatism in the North American Cordillera: The temporal and spatial association of magmatism and metamorphic core complexes, *J. Geophys. Res.*, *96*, 13,201–13,224, doi:10.1029/91JB00412.

Asimow, P. D., J. E. Dixon, and C. H. Langmuir (2004), A hydrous melting and fractionation model for mid-ocean ridge basalts: Application to the Mid-Atlantic Ridge near the Azores, *Geochem. Geophys. Geosyst.*, *5*, Q01E16, doi:10.1029/2003GC000568.

Axen, G. J., J. Selverstone, T. Byrne, and J. M. Fletcher (1998), If the strong crust leads, will the weak crust follow?, *GSA Today*, *8*(12), 1–8.

Bailey, C. M., M. S. Harris, and D. W. Marchetti (2007), Geologic overview of the Fish Lake plateau, Utah, in *Central Utah—Diverse Geology of a Dynamic Landscape*, edited by G. C. Willis et al., *Utah Geol. Assoc. Publ. 36*, pp. 45–55, Salt Lake City.

Bailey, R. C. (1990), Trapping of aqueous fluids in the deep crust, *Geophys. Res. Lett.*, *17*, 1129–1132, doi:10.1029/GL017i008p01129.

Batschelet, E. (1981), *Circular Statistics in Biology*, 371 pp., Academic, London.

Best, M. G., E. H. McKee, and P. E. Damon (1980), Space-time-composition patterns of Late Cenozoic mafic volcanism, southwestern Utah and adjoining areas, *Am. J. Sci.*, *280*, 1035–1050.

Bodell, J. M., and D. S. Chapman (1982), Heat flow in the north-central Colorado Plateau, *J. Geophys. Res.*, *87*, 2869–2884, doi:10.1029/JB087iB04p02869.

Boyd, O. S., and A. F. Sheehan (2005), Attenuation tomography beneath the Rocky Mountain Front: Implications for the physical state of the upper mantle, in *The Rocky Mountain Region: An Evolving Lithosphere*, *Geophys. Monogr. Ser.*, vol. 154, edited by R. G. Keller, pp. 361–377, AGU, Washington, D. C.

Burchfiel, B. C., D. S. Cowan, and G. A. Davis (1992), Tectonic overview of the Cordilleran orogen in the western United States, in *The Geology of North America*, vol. G-3, *The Cordilleran Orogen: Coterminous U.S.*, edited by B. C. Burchfiel, P. W. Lipman, and M. L. Zoback, pp. 407–480, Geol. Soc. of Am., Boulder, Colo.

Bureau, H., and H. Keppler (1999), Complete miscibility between silicate melts and hydrous fluids in the upper mantle: Experimental evidence and geochemical implications, *Earth Planet. Sci. Lett.*, *165*, 187–196, doi:10.1016/S0012-821X(98)00266-0.

Caldwell, T. G., H. M. Bibby, and C. Brown (2004), The magnetotelluric phase tensor, *Geophys. J. Int.*, *158*, 457–469, doi:10.1111/j.1365-246X.2004.02281.x.

Carmichael, I. S. E. (1991), The redox states of basic and silicic magmas: A reflection of their source regions?, *Contrib. Mineral. Petrol.*, *106*, 129–141, doi:10.1007/BF00306429.

Chapman, D. S., M. D. Clement, and C. W. Mase (1981), Thermal regime of the Escalante Desert, Utah, with an analysis of the Newcastle geothermal system, *J. Geophys. Res.*, *86*, 11,735–11,746, doi:10.1029/JB086iB12p11735.

Christiansen, E. H., M. F. Sheridan, and D. M. Burt (1986), The geology and geochemistry of Cenozoic topaz rhyolites from the western United States, *Geol. Soc. Am. Spec. Pap.*, *205*, 82 pp.

Christiansen, E. H., I. Haapala, and G. L. Hart (2007), Are Cenozoic topaz rhyolites the erupted equivalents of Proterozoic rapakivi granites? Examples from the western United States and Finland, *Lithos*, *97*, 219–246, doi:10.1016/j.lithos.2007.01.010.

Christiansen, R. L., and E. H. McKee (1978), Late Cenozoic volcanic and tectonic evolution of the Great Basin and Columbia intermontane regions, in *Cenozoic Tectonics and Regional Geophysics of the Western Cordillera*, edited by R. B. Smith and G. P. Eaton, *Mem.Geol. Soc. Am.*, *152*, 283–312.

Christiansen, R. L., and R. S. Yeats (1992), Post-Laramide geology of the U.S. Cordilleran region, in *The Geology of North America*, vol. G-3, *The Cordilleran Orogen: Coterminous U.S.*, edited by B. C. Burchfiel, P. W. Lipman, and M. L. Zoback, pp. 261–406, Geol. Soc. of Am., Boulder, Colo.

Clemens, J. D., and J. M. Watkins (2001), The fluid regime of high-temperature metamorphism during granitoic magma genesis, *Contrib. Mineral. Petrol.*, *140*, 600–606.

Coleman, D. S., and J. D. Walker (1992), Evidence for the generation of juvenile granitic crust during continental extension, Mineral Mountains batholith, Utah, *J. Geophys. Res.*, *97*, 11,011–11,024, doi:10.1029/92JB00653.

Coleman, D. S., J. M. Bartley, J. D. Walker, D. E. Price, and A. M. Friedrich (1997), Extensional faulting, footwall deformation and plutonism in the Mineral Mountains, Southern Sevier Desert, in *Mesozoic to Recent Geology of Utah (Field Trip Guidebook, 1997 GSA Annual Meeting)*, edited by P. Link and B. Kowallis, *Brigham Young Univ. Geol. Stud.*, *42*(2), pp. 203–233, Provo, Utah.

Constable, S. (2006), SEO3: A new model of olivine electrical conductivity, *Geophys. J. Int.*, *166*, 435–437, doi:10.1111/j.1365-246X.2006.03041.x.

Constenius, K. N. (1996), Late Paleogene extensional collapse of the Cordilleran foreland fold and thrust belt, *Geol. Soc. Am. Bull.*, *108*, 20–39, doi:10.1130/0016-7606(1996)108<0020:LPECOT>2.3.CO;2.

Coolbaugh, M., G. Arehart, J. Faulds, L. Garside, and L. Shevenell (2005a), Active geothermal systems and associated gold deposits in the Great Basin, *Trans. Geotherm. Resour. Counc.*, *29*, 215–221.

Coolbaugh, M., G. Arehart, J. Faulds, and L. Garside (2005b), Geothermal systems in the Great Basin, western United States: Modern analogs to the roles of magmatism, structure, and regional tectonics in the formation of gold deposits, in *Geological Society of Nevada Symposium 2005: Windows to the World*, edited by H. N. Rhoden, R. C. Steininger, and P. G. Vikre, pp. 1063–1081, Geol. Soc. of Nev., Reno.

Crossey, L. J., T. B. Fischer, P. J. Patchett, K. E. Karlstrom, D. R. Hilton, D. L. Newell, P. Huntoon, and A. C. Reynolds (2006), Dissected hydrologic system at the Grand Canyon: Interaction between deeply derived fluids and plateau aquifer waters in modern springs and travertine, *Geology*, *34*, 25–28, doi:10.1130/G22057.1.

Crowley, J. L., M. D. Schmitz, S. A. Bowring, M. L. Williams, and K. E. Karlstrom (2006), U-Pb and Hf isotopic analysis of zircon in lower crustal xenoliths from the Navajo volcanic field: 1.4 Ga mafic magmatism and metamorphism beneath the Colorado Plateau, *Contrib. Mineral. Petrol.*, *151*, 313–330, doi:10.1007/s00410-006-0061-z.

Cunningham, C. G., R. O. Rye, B. W. Rockwell, M. J. Kunk, and T. B. Councell (2005), Supergene destruction of a hydrothermal replacement alunite deposit at Big Rock Candy Mountain, Utah: Mineralogy, spectroscopic remote sensing, stable-isotope, and argon-age evidences, *Chem. Geol.*, *215*, 317–337, doi:10.1016/j.chemgeo.2004.06.055.

Cunningham, C. G., P. D. Rowley, T. A. Steven, and R. O. Rye (2007), Geologic evolution and mineral resources of the Marysvale volcanic field, west-central Utah, in *Central Utah—Diverse Geology of a Dynamic Landscape*, edited by G. C. Willis et al., *Utah Geol. Assoc. Publ. 36*, pp. 143–162, Salt Lake City.

Davis, M., and N. J. Kuznir (2004), Depth-dependent lithospheric stretching at rifted continental margins, in *Proceedings of the NSF Rifted Margins Theoretical Institute*, edited by G. D. Karner, pp. 92–136, Columbia Univ. Press, New York.

DeCelles, P. G. (2004), Late Jurassic to Eocene evolution of the Cordilleran thrust belt and foreland basin system, western U.S.A., *Am. J. Sci.*, *304*, 105–168, doi:10.2475/ajs.304.2.105.

DeCelles, P. G., and J. C. Coogan (2006), Regional structure and kinematic history of the Sevier fold-and-thrust belt, central Utah, *Geol. Soc. Am. Bull.*, *118*, 841–864, doi:10.1130/B25759.1.

DeGroot-Hedlin, C. M., and S. C. Constable (1990), Occam's inversion to generate smooth, two-dimensional models from magnetotelluric data, *Geophysics*, *55*, 1613–1624, doi:10.1190/1.1442813.

DePaolo, D. J., and E. E. Daley (2000), Neodymium isotopes in basalts of the southwest Basin and Range and lithospheric thinning during continental extension, *Chem. Geol.*, *169*, 157–185, doi:10.1016/S0009-2541(00)00261-8.

Dickinson, W. R., and T. F. Lawton (2003), Sequential intercontinental suturing as the ultimate control for Pennsylvanian Ancestral Rocky Mountains deformation, *Geology*, *31*, 609–612, doi:10.1130/0091-7613(2003)031<0609:SISATU>2.0.CO;2.

Duba, A. G., and S. C. Constable (1993), The electrical conductivity of lherzolite, *J. Geophys. Res.*, *98*, 11,885–11,899, doi:10.1029/93JB00995.

Ducea, M. N., and J. B. Saleeby (1998), A case for delamination of the deep batholithic crust beneath the Sierra Nevada, California, *Int. Geol. Rev.*, *133*, 78–93.

Duebendorfer, E. M., K. R. Chamberlain, and B. Fry (2006), Mojave-Yavapai boundary zone, southwestern United States: A rifting model for the formation of an isotopically mixed crustal boundary zone, *Geology*, *34*, 681–684, doi:10.1130/G22581.1.

Dumitru, T. A., P. B. Gans, D. A. Foster, and E. L. Miller (1991), Refrigeration of the western Cordilleran lithosphere during Laramide shallow-angle subduction, *Geology*, *19*, 1145–1148, doi:10.1130/0091-7613(1991)019<1145:ROTWCL>2.3.CO;2.

Dumitru, T. A., E. L. Miller, B. E. Surpless, C. M. Martinez, A. E. Egger, and D. Stockli (2000), Large structural domains of synchronous Miocene extension in the northern Basin and Range Province, *Geol. Soc. Am. Abstr. Programs*, *32*(7), A43.

Eaton, G. P., R. R. Wahl, H. J. Prostka, D. R. Mabey, and M. D. Kleinkopf (1978), Regional gravity and tectonic patterns: Their relation to late Cenozoic epeirogeny and lateral spreading in the western Cordillera, in *Cenozoic Tectonics and Regional Geophysics of the Western Cordillera*, edited by R. B. Smith and G. P. Eaton, *Mem. Geol. Soc. Am.*, *152*, 61–91.

Egbert, G. D., and J. R. Booker (1986), Robust estimation of geomagnetic transfers functions, *Geophys. J. R. Astron. Soc.*, *87*, 173–194.

Egbert, G. D., and D. W. Livelybrook (1996), Single station magnetotelluric impedance estimation: Coherence weighting and the regression M-estimate, *Geophysics*, *61*, 964–970, doi:10.1190/1.1444045.

Evans, R. L., G. Hirth, K. Baba, D. Forsyth, A. Chave, and R. Mackie (2005), Geophysical evidence from the MELT area for compositional controls on oceanic plates, *Nature*, *437*, 249–252, doi:10.1038/nature04014.

Farmer, G. L., A. F. Glazner, and C. R. Manley (2002), Did lithospheric delamination trigger late Cenozoic potassic volcanism in the southern Sierra Nevada, California?, *Geol. Soc. Am. Bull.*, *114*, 754–768, doi:10.1130/0016-7606(2002)114<0754:DLDTLC>2.0.CO;2.

Flesch, L. M., W. E. Holt, A. J. Haines, L. Wen, and B. Shen-Tu (2007), The dynamics of western North America: Stress magnitudes and the relative role of gravitational potential energy, plate interaction at the boundary and basal traction, *Geophys. J. Int.*, *169*, 866–896, doi:10.1111/j.1365-246X.2007.03274.x.

Fournier, R. O. (1999), Hydrothermal processes related to movement of fluid from plastic into brittle rock in the magmatic-epithermal environment, *Econ. Geol.*, *94*, 1193–1212.

Frost, B. R., C. D. Frost, and J. L. R. Touret (1989), Magmas as a source of heat and fluids in granulite metamorphism, in *Fluid Movements—Elemental Transport and the Composition of the Deep Crust*, edited by D. Bridgwater, *NATO ASI Ser., Ser. C*, *281*, 1–18.

Gaillard, F. (2004), Laboratory measurements of electrical conductivity of hydrous and dry silicate melts under pressure, *Earth Planet. Sci. Lett.*, *218*, 215–228, doi:10.1016/S0012-821X(03)00639-3.

Gamble, T., W. Goubau, and J. Clarke (1979), Magnetotellurics with a remote reference, *Geophysics*, *44*, 53–68, doi:10.1190/1.1440923.

Gernigon, L., F. Lucazeau, F. Brigaud, J.-C. Ringenbach, S. Planke, and B. Le Gall (2006), A moderate melting model for the Voring margin (Norway) based on structural observations and a thermo-kinematical modeling: implication for the meaning of the lower crustal bodies, *Tectonophysics*, *412*, 255–278, doi:10.1016/j.tecto.2005.10.038.

Gibson, S. A., R. N. Thompson, P. T. Leat, M. A. Morrison, G. L. Hendry, A. P. Dickin, and J. G. Mitchell (1993), Ultrapotassic magmas along the flanks of the Oligo-Miocene Rio Grande Rift, USA: Monitors of the zone of lithospheric mantle extension and thinning beneath a continental rift, *J. Petrol.*, *34*, 187–228.

Gilbert, H. J., and A. F. Sheehan (2004), Images of crustal variations in the intermountain west, *J. Geophys. Res.*, *109*, B03306, doi:10.1029/2003JB002730.

Goes, S., and S. van der Lee (2002), Thermal structure of the North American uppermost mantle inferred from seismic tomography, *J. Geophys. Res.*, *107*(B3), 2050, doi:10.1029/2000JB000049.

Gough, D. I. (1989), Magnetometer array studies, earth structure, and tectonic processes, *Rev. Geophys.*, *27*, 141–157, doi:10.1029/RG027i001p00141.

Grant, F. S., and G. F. West (1965), *Interpretation Theory in Applied Geophysics*, 584 pp., McGraw-Hill, New York.

Haak, V., and R. Hutton (1986), Electrical resistivity in continental lower crust, in *Nature of Lower Continental Crust*, edited by J. B. Dawson et al., *Geol. Soc. Spec. Publ.*, *24*, 35–49.

Hammond, W. C. (2005), The ghost of an earthquake, *Science*, *310*, 1440–1442, doi:10.1126/science.1121349.

Hammond, W. C., and W. Thatcher (2004), Contemporary tectonic deformation of the Basin and Range province, western United States: 10 years of observation with the Global Positioning System, *J. Geophys. Res.*, *109*, B08403, doi:10.1029/2003JB002746.

Hammond, W. C., and W. Thatcher (2005), Northwest Basin and Range tectonic deformation observed with the Global Positioning System, 1999–2003, *J. Geophys. Res.*, *110*, B10405, doi:10.1029/2005JB003678.

Hawkesworth, C., S. Turner, K. Gallagher, A. Hunter, T. Bradshaw, and N. Rogers (1995), Calc-alkaline magmatism, lithospheric thinning and extension in the Basin and Range, *J. Geophys. Res.*, *100*, 10,271–10,286, doi:10.1029/94JB02508.

Heise, W., and J. Pous (2001), Effects of anisotropy on the two-dimensional inversion procedure, *Geophys. J. Int.*, *147*, 610–621, doi:10.1046/j.0956-540x.2001.01560.x.

Herzberg, C., P. D. Asimow, N. Arndt, Y. Niu, C. M. Lesher, J. G. Fitton, M. J. Cheadle, and A. D. Saunders (2007), Temperatures in ambient mantle and plumes: Constraints from basalts, picrites, and komatiites, *Geochem. Geophys. Geosyst.*, *8*, Q02006, doi:10.1029/2006GC001390.

Hintze, L. F. (1980), Geologic map of Utah, scale 1:500,000, Utah Geol. Mineral. Surv., Salt Lake City.

Hintze, L. F. (1988), Geologic history of Utah, *Brigham Young Univ. Geol. Stud. Spec. Publ. 7*, 202 pp., Provo, Utah.

Hohmann, G. W., and A. P. Raiche (1988), Inversion of controlled source electromagnetic data, in *Electromagnetic Methods in Applied Geophysics*, edited by M. N. Nabighian, pp. 443–468, Soc. of Explor. Geophys., Tulsa, Okla.

Holness, M. B. (1996), Surface chemical controls on pore-fluid connectivity in texturally equilibrated materials, in *Fluid Flow and Transport in Rocks*, edited by B. Jamveit and B. Yardley, pp. 149–169, Chapman & Hall, London.

Holness, M. B. (1997), The permeability of non-deforming rock, in *Deformation-Enhanced Fluid Transport in the Earth's Crust and Mantle*, edited by M. B. Holness, pp. 9–39, Chapman & Hall, London.

Holtzman, B. K., and D. L. Kohlstedt (2007), Stress-driven melt segregation and strain partitioning in partially molten rocks: Effects of stress and strain, *J. Petrol.*, *48*, 2379–2406, doi:10.1093/petrology/egm065.

Holtzman, B. K., D. L. Kohlstedt, M. E. Zimmerman, F. Heidelbach, T. Hiraga, and J. Hustoft (2003), Melt segregation and strain partitioning: Implications for seismic anisotropy and mantle flow, *Science*, *301*, 1227–1230, doi:10.1126/science.1087132.

Humphreys, E. D. (1995), Post-Laramide removal of the Farallon slab, western United States, *Geology*, *23*, 987–990, doi:10.1130/0091-7613(1995)023<0987:PLROTF>2.3.CO;2.

Humphreys, E. D., and K. G. Dueker (1994), Physical state of the western U.S. mantle, *J. Geophys. Res.*, *99*, 9635–9650, doi:10.1029/93JB02640.

Humphreys, E. D., E. Hessler, K. Dueker, E. Erslev, G. L. Farmer, and T. Atwater (2003), How Laramide-age hydration of North America by the Farallon slab controlled subsequent activity in the western U.S., *Int. Geol. Rev.*, *45*, 575–595, doi:10.2747/0020-6814.45.7.575.

Hyndman, R. D., L. L. Vanyan, G. Marquis, and L. K. Law (1993), The origin of electrically conductive lower continental crust: Saline water or graphite?, *Phys. Earth Planet. Inter.*, *81*, 325–344, doi:10.1016/0031-9201(93)90139-Z.

Jiracek, G. R., V. Haak, and K. H. Olsen (1995), Practical magnetotellurics in a continental rift environment, in *Continental Rifts: Evolution, Structure and Tectonics*, edited by K. H. Olsen, pp. 103–129, Elsevier, New York.

John, D. (2001), Miocene and early Pliocene epithermal gold-silver deposits in the northern Great Basin, western United States: Characteristics, distribution, and relationship to magmatism, *Econ. Geol.*, *96*, 1827–1853, doi:10.2113/96.8.1827.

Johnson, K. R., D. Schelling, and D. Wavrek (2007), Covenant Field: A major oil discovery in the Sevier thrust belt of central Utah, *Leading Edge*, *26*(2), 168–171, doi:10.1190/1.2542445.

Jones, A. G. (1983), The problem of current-channeling: A critical review, *Geophys. Surv.*, *6*, 79–122, doi:10.1007/BF01453996.

Jones, A. G. (1992), Electrical conductivity of the continental lower crust, in *Continental Lower Crust*, edited by D. M. Fountain, R. J. Arculus, and R. W. Kay, pp. 81–143, Elsevier, Amsterdam.

Jones, A. G. (1999), Imaging the continental upper mantle using electromagnetic methods, *Lithos*, *48*, 57–58, doi:10.1016/S0024-4937(99)00022-5.

Jones, A. G., A. D. Chave, G. Egbert, D. Auld, and K. Bahr (1989), A comparison of techniques for magnetotelluric response function estimation, *J. Geophys. Res.*, *94*, 14,201–14,213, doi:10.1029/JB094iB10p14201.

Jones, C. H., and R. A. Phinney (1998), Seismic structure of the lithosphere from teleseismic converted arrivals observed at small arrays in the southern Sierra Nevada and vicinity, California, *J. Geophys. Res.*, *103*, 10,065–10,090, doi:10.1029/97JB03540.

Jones, C. H., H. Kanamori, and S. W. Roecker (1994), Missing roots and mantle "drips": Regional Pn and teleseismic arrival times in the southern Sierra Nevada and vicinity, California, *J. Geophys. Res.*, *99*, 4567–4601, doi:10.1029/93JB01232.

Jones, C. H., G. L. Farmer, and J. Unruh (2004), Tectonics of Pliocene removal of lithosphere of the Sierra Nevada, Cali-

fornia, *Geol. Soc. Am. Bull.*, *116*, 1408–1422, doi:10.1130/B25397.1.

Karato, S. (1990), The role of hydrogen in the electrical conductivity of the upper mantle, *Nature*, *347*, 272–273, doi:10.1038/347272a0.

Karato, S., and H.-R. Wenk (2002), *Plastic Deformation of Minerals and Rocks*, *Rev. Mineral. Geochem.*, vol. 51, 420 pp., Mineral. Soc. of Am., Washington, D. C.

Kariya, K. A., and T. J. Shankland (1983), Electrical conductivity of dry lower crustal rocks, *Geophysics*, *48*, 52–61, doi:10.1190/1.1441407.

Karlstrom, K. E., S. S. Harlan, M. L. Williams, J. McLelland, J. W. Geissman, and K.-I. Ahall (1999), Redefining Rodinia: Geologic evidence for the Australia-western U.S. connection in the Proterozoic, *GSA Today*, *9*(10), 1–7.

Karlstrom, K. E., K.-I. Ahall, S. S. Harlan, M. L. Williams, J. McLelland, and J. W. Geissman (2001), Long-lived (1.8–1.0 Ga) convergent orogen in southern Laurentia, its extensions to Australia and Baltica, and implications for refining Rodinia, *Precambrian Res.*, *111*, 5–30, doi:10.1016/S0301-9268(01)00154-1.

Katz, R. F., M. Spiegelman, and B. Holtzman (2006), The dynamics of melt and shear localization in partially molten aggregates, *Nature*, *442*, 676–679, doi:10.1038/nature05039.

Keller, G. R., R. B. Smith, and L. W. Braile (1975), Crustal structure along the Great Basin-Colorado Plateau transition from seismic refraction studies, *J. Geophys. Res.*, *80*, 1093–1098, doi:10.1029/JB080i008p01093.

Kelley, K. A., T. Plank, T. L. Grove, E. M. Stolper, S. Newman, and E. Hauri (2006), Mantle melting as a function of water content beneath back-arc basins, *J. Geophys. Res.*, *111*, B09208, doi:10.1029/2005JB003732.

Kempton, P. D., J. G. Fitton, C. J. Hawkesworth, and D. S. Ormerod (1991), Isotopic and trace element constraints on the composition and evolution of the lithosphere beneath the southwestern United States, *J. Geophys. Res.*, *96*, 13,713–13,735, doi:10.1029/91JB00373.

Kendall, J.-M. (1994), Teleseismic arrivals at a mid-ocean ridge: effects of mantle melt and anisotropy, *Geophys. Res. Lett.*, *21*, 301–304, doi:10.1029/93GL02791.

Kennedy, B. M., and M. C. van Soest (2006), A helium isotope perspective on the Dixie Valley, Nevada, hydrothermal system, *Geothermics*, *35*, 26–43, doi:10.1016/j.geothermics.2005.09.004.

Kennedy, B. M., and M. C. van Soest (2007), Flow of mantle fluids through the ductile lower crust: Helium isotope trends, *Science*, *318*, 1433–1436.

Kilty, K., D. S. Chapman, and C. W. Mase (1979), Forced convective heat transfer in the Monroe Hot Springs geothermal system, *J. Volcanol. Geotherm. Res.*, *6*, 257–277, doi:10.1016/0377-0273(79)90005-2.

Korenaga, J., P. B. Kelemen, and W. S. Holbrook (2002), Methods for resolving the origin of large igneous provinces from crustal seismology, *J. Geophys. Res.*, *107*(B9), 2178, doi:10.1029/2001JB001030.

Kuznir, N. J., R. Hunsdale, A. M. Roberts, and SIMM Team (2005), Norwegian margin depth-dependent stretching, in *Petroleum Geology: Northwest Europe and Global Perspectives, Proceedings of the 6th Petroleum Geology Conference*, edited by A. G. Dore and B. A. Vining, pp. 767–783, Geol. Soc. of London.

Lachenbruch, A. H., and J. H. Sass (1978), Models of an extending lithosphere and heat flow in the Basin and Range province, in *Cenozoic Tectonic and Regional Geophysics of the Western Cordillera*, edited by R. B. Smith and G. P. Eaton, *Mem. Geol. Soc. Am.*, *152*, 209–250.

Laporte, D. (1994), Wetting behavior of partial melts during crustal anatexis: The distribution of hydrous silicic melts in polycrystalline aggregates of quartz, *Contrib. Mineral. Petrol.*, *116*, 486–499, doi:10.1007/BF00310914.

Larsen, J. C., R. L. Mackie, A. Manzella, A. Fiordelisi, and S. Rieven (1996), Robust, smooth magnetotelluric transfer functions, *Geophys. J. R. Astron. Soc.*, *124*, 801–819.

Lastowka, L. A., A. F. Sheehan, and J. N. Schneider (2001), Seismic evidence for partial lithospheric delamination model of Colorado Plateau uplift, *Geophys. Res. Lett.*, *28*, 1319–1322, doi:10.1029/2000GL012360.

Ledo, J. (2005), 2-D versus 3-D magnetotelluric data interpretation, *Surv. Geophys.*, *26*, 511–543, doi:10.1007/s10712-005-1757-8.

Lee, C.-T., Q. Yin, R. L. Rudnick, and S. B. Jacobsen (2001), Preservation of ancient and fertile lithospheric mantle beneath the southwestern United States, *Nature*, *411*, 69–73, doi:10.1038/35075048.

Lizarralde, D., A. Chave, G. Hirth, and A. Schultz (1995), Northeastern Pacific mantle conductivity profile from long-period magnetotelluric sounding using Hawaii-to-California submarine cable data, *J. Geophys. Res.*, *100*, 17,837–17,854, doi:10.1029/95JB01244.

Loeb, D. T., and J. C. Pechmann (1986), The P wave velocity structure of the crust-mantle boundary beneath Utah from network travel-time measurements (abstract), *Earthquake Notes*, *57*, 10–11.

Lowry, A. R., N. M. Ribe, and R. B. Smith (2000), Dynamic elevation of the Cordillera, western United States, *J. Geophys. Res.*, *105*, 23,371–23,390, doi:10.1029/2000JB900182.

Mackie, R. L., L. Bennett, and T. R. Madden (1988), Long period magnetotelluric measurements near the central California coast: A land-locked view of the conductivity structure under the Pacific Ocean, *Geophys. J. Int.*, *95*, 181–194, doi:10.1111/j.1365-246X.1988.tb00459.x.

McCammon, C. (2005), The paradox of mantle redox, *Science*, *308*, 807–808, doi:10.1126/science.1110532.

McKenzie, D. P. (1978), Some remarks on the development of sedimentary basins, *Earth Planet. Sci. Lett.*, *40*, 25–32, doi:10.1016/0012-821X(78)90071-7.

McQuarrie, N., and C. Chase (2000), Raising the Colorado Plateau, *Geology*, *28*, 91–94, doi:10.1130/0091-7613(2000)028<0091:RTCP>2.0.CO;2.

Mibe, K., T. Fujii, and A. Yasuda (1998), Connectivity of aqueous fluid in the Earth's upper mantle, *Geophys. Res. Lett.*, *25*, 1233–1236, doi:10.1029/98GL00872.

Miller, D. M., T. H. Nilsen, and W. L. Bilodeau (1992), Late Cretaceous to early Eocene geologic evolution of the U.S. Cordillera, in *The Geology of North America*, vol. G-3, *The Cordilleran Orogen: Coterminous U.S.*, edited by B. C. Burchfiel, P. W. Lipman, and M. L. Zoback, pp. 205–260, Geol. Soc. of Am., Boulder, Colo.

Miller, E. L., T. A. Dumitru, R. W. Brown, and P. B. Gans (1999), Rapid Miocene slip on the Snake Range-Deep Creek Range fault system, east-central Nevada, *Geol. Soc. Am. Bull.*, *111*, 886–905, doi:10.1130/0016-7606(1999)111<0886:RMSOTS>2.3.CO;2.

Nagel, T. J., and W. R. Buck (2004), Symmetric alternative to asymmetric rifting models, *Geology*, *32*, 937–940, doi:10.1130/G20785.1.

Nagel, T. J., and W. R. Buck (2007), Control of rheological stratification on rifting geometry: A symmetric rift model resolving the upper plate paradox, *Int. J. Earth Sci.*, *96*(6), 1047–1057, doi:10.1007/s00531-007-0195-x.

Nelson, S. T., and J. P. Davidson (1993), Interactions between mantle-derived magmas and mafic crust, Henry Mountains, Utah, *J. Geophys. Res.*, *98*, 1837–1852, doi:10.1029/92JB02689.

Nelson, S. T., and R. A. Harris (2001), The role of rheology in the tectonic history of the Colorado Plateau, in *The Geological Transition: Colorado Plateau to Basin and Range, Proceedings of the J. Hoover Mackin Symposium*, *Cedar City, Utah, September 20–23, UGA/AAPG Guideb. 30/GB78*, edited by M. C. Erskine et al., pp. 189–203, Utah Geol. Surv., Salt Lake City.

Nelson, S. T., and D. G. Tingey (1997), Time-transgressive and extension-related basaltic volcanism in southwest Utah and vicinity, *Geol. Soc. Am. Bull.*, *109*, 1249–1265, doi:10.1130/0016-7606(1997)109<1249:TTAERB>2.3.CO;2.

Nelson, S. T., R. A. Harris, M. J. Dorais, and M. Heizler (2002), Basement complexes in the Wasatch fault, Utah, provide new limits on crustal accretion, *Geology*, *30*, 831–834, doi:10.1130/0091-7613(2002)030<0831:BCITWF>2.0.CO;2.

Nesbitt, B. E. (1993), Electrical resistivities of crustal fluids, *J. Geophys. Res.*, *98*, 4301–4310, doi:10.1029/92JB02576.

Newell, D. L., L. J. Crossey, K. Karlstrom, T. Fischer, and D. Hilton (2005), Evidence for continental-scale links between the mantle and groundwater systems of the western United States based on hydrogeochemistry of travertine-depositing springs and regional synthesis of helium isotopic data, *GSA Today*, *15*(12), 4–10, doi:10.1130/1052-5173(2005)015[4:CSLBTM]2.0.CO;2.

Nielson, D. L., S. H. Evans, Jr., and B. S. Sibbett (1986), Magmatic, structural, and hydrothermal evolution of the Mineral Mountains intrusive complex, Utah, *Geol. Soc. Am. Bull.*, *97*, 765–777, doi:10.1130/0016-7606(1986)97<765:MSAHEO>2.0.CO;2.

Niemi, N. A., B. P. Wernicke, A. M. Friedrich, M. Simons, R. A. Bennett, and J. L. Davis (2004), BARGEN continuous GPS data across the eastern Basin and Range province, and implications for fault system dynamics, *Geophys. J. Int.*, *159*, 842–862, doi:10.1111/j.1365-246X.2004.02454.x.

Pakiser, L. C. (1989), Geophysics of the intermontane system, in *Geophysical Framework of the Continental United States*, edited by L. C. Pakiser and W. D. Mooney, *Mem. Geol. Soc. Am.*, *172*, 235–247.

Park, S. K. (2004), Mantle heterogeneity beneath eastern California from magnetotelluric measurements, *J. Geophys. Res.*, *109*, B09406, doi:10.1029/2003JB002948.

Park, S. K., and B. Wernicke (2003), Electrical conductivity images of Quaternary faults and Tertiary detachments in the California Basin and Range, *Tectonics*, *22*(4), 1030, doi:10.1029/2001TC001324.

Park, S. K., G. P. Biasi, R. L. Mackie, and T. R. Madden (1991), Magnetotelluric evidence of crustal suture zones bounding the southern Great Valley, California, *J. Geophys. Res.*, *96*, 353–376, doi:10.1029/90JB02078.

Park, S. K., B. Hirasuna, G. R. Jiracek, and C. Kinn (1996), Magnetotelluric evidence of lithospheric mantle thinning beneath the southern Sierra Nevada, *J. Geophys. Res.*, *101*, 16,241–16,255, doi:10.1029/96JB01211.

Parkinson, I. J., and R. J. Arculus (1999), The redox state of subduction zones: Insights from arc-peridotites, *Chem. Geol.*, *160*, 409–423, doi:10.1016/S0009-2541(99)00110-2.

Pastana de Lugão, P., and P. E. Wannamaker (1996), Calculating the two-dimensional magnetotelluric Jacobian in finite elements using reciprocity, *Geophys. J. Int.*, *127*, 806–810, doi:10.1111/j.1365-246X.1996.tb04060.x.

Perry, F. V., D. J. DePaolo, and W. S. Baldridge (1993), Neodymium isotopic evidence for decreasing crustal contributions to Cenozoic ignimbrites of the western United States: Implications for the thermal evolution of the Cordilleran crust, *Geol. Soc. Am. Bull.*, *105*, 872–882, doi:10.1130/0016-7606(1993)105<0872:NIEFDC>2.3.CO;2.

Poe, B., C. Romano, F. Nestola, and D. Rubie (2005), Electrical conductivity of hydrous single crystal olivine, *Eos Trans. AGU*, *86*(52), Fall Meet. Suppl., Abstract MR41A-0895.

Porath, H. (1971), Magnetic variation anomalies and seismic low-velocity zone in the western United States, *J. Geophys. Res.*, *76*, 2643–2648, doi:10.1029/JB076i011p02643.

Porath, H., D. W. Oldenburg, and D. I. Gough (1970), Separation of magnetic variation fields and conductive structures in the western United States, *Geophys. J. R. Astron. Soc.*, *19*, 237–260.

Riciputi, L. R., C. M. Johnson, D. A. Sawyer, and P. W. Lipman (1995), Crustal and magmatic evolution in a large multicyclic caldera complex: Isotopic evidence from the central San Juan volcanic field, *J. Volcanol. Geotherm. Res.*, *67*, 1–28, doi:10.1016/0377-0273(94)00097-Z.

Roberts, J. J., and J. A. Tyburczy (1999), Partial-melt electrical conductivity: Influence of melt composition, *J. Geophys. Res.*, *104*, 7055–7065, doi:10.1029/1998JB900111.

Rockwell, B. W., C. G. Cunningham, G. N. Breit, and R. O. Rye (2006), Spectroscopic mapping of the Whitehorse alunite deposit, Marysvale volcanic field, Utah: Evidence of a magmatic component, *Econ. Geol.*, *101*, 1377–1395, doi:10.2113/gsecongeo.101.7.1377.

Rodi, W. L., and R. L. Mackie (2001), Nonlinear conjugate gradients algorithm for 2-D magnetotelluric inversion, *Geophysics*, *66*, 174–187, doi:10.1190/1.1444893.

Ross, H. P., and J. N. Moore (1985), Geophysical investigations of the Cove Fort-Sulphurdale geothermal system, Utah, *Geophysics*, *50*, 1732–1745, doi:10.1190/1.1441863.

Rowley, P. D. (1998), Cenozoic transverse zones and igneous belts in the Great Basin, western United States: Their tectonic and economic implications, in *Accommodation Zones and Transfer Zones: The Regional Segmentation of the Basin and Range Province*, edited by J. E. Faulds and Stewart, *Spec. Pap. Geol. Soc. Am.*, *323*, 195–228.

Rowley, P. D., T. A. Steven, J. J. Anderson, and C. G. Cunningham (1979), Cenozoic stratigraphic and structural framework of southwestern Utah, *U.S. Geol. Surv. Prof. Pap.*, *1149*, 22 pp.

Rowley, P. D., T. A. Steven, and H. H. Mehnert (1981), Origin and structural implications of upper Miocene rhyolites in Kingston Canyon, Piute County, Utah, *Geol. Soc. Am. Bull.*, *92*, 590–602, doi:10.1130/00167606(1981)92<590:OASIOU>2.0.CO;2.

Rowley, P. D., C. G. Cunningham, T. A. Steven, H. H. Mehnert, and C. W. Naeser (1998), Cenozoic igneous and tectonic setting of the Marysvale volcanic field and its relation to other igneous centers in Utah and Nevada, in *Laccolith Complexes of Southeastern Utah: Time of Emplacement and Tectonic Setting*, edited by J. D. Friedman and A. C. J. Huffman, *U.S. Geol. Surv. Bull.*, *2158*, 167–201.

Royse, F.Jr. (1993), Case of the phantom foredeep: Early Cretaceous in west-central Utah, *Geology*, *21*, 133–136, doi:10.1130/0091-7613(1993)021<0133:COTPFE>2.3.CO;2.

Rudnick, R. L., and D. M. Fountain (1995), Nature and composition of the continental crust: a lower crustal perspective, *Rev. Geophys.*, *33*, 267–309, doi:10.1029/95RG01302.

Ruppel, C. (1995), Extensional processes in continental lithosphere, *J. Geophys. Res.*, *100*, 24,187–24,215, doi:10.1029/95JB02955.

Sahagian, D., A. Proussevitch, and W. Carlson (2002), Timing of Colorado Plateau uplift: Initial constraints from vesicular basalt-derived paleoelevations, *Geology*, *30*, 807–810, doi:10.1130/0091-7613(2002)030<0807:TOCPUI>2.0.CO;2.

Schelling, D. D., D. Strickland, K. Johnson, and J. Vrona (2007), Structural geology of the central Utah thrust belt, in *Central Utah—Diverse Geology of a Dynamic Landscape*, edited by G. C. Willis et al., *Utah Geol. Assoc. Publ. 36*, pp. 1–29, Salt Lake City.

Shankland, T. J., and M. E. Ander (1983), Electrical conductivity, temperature, and fluids in the lower crust, *J. Geophys. Res.*, *88*, 9475–9484, doi:10.1029/JB088iB11p09475.

Sheehan, A. F., C. H. Jones, M. K. Savage, S. Ozalaybey, and J. M. Schneider (1997), Contrasting lithospheric structure between the Colorado Plateau and Great Basin: initial results from Colorado Plateau-Great Basin PASSCAL experiment, *Geophys. Res. Lett.*, *24*, 2609–2612, doi:10.1029/97GL02782.

Shuey, R. T., D. K. Schellinger, E. H. Johnson, and L. B. Alley (1973), Aeromagnetics and the transition between the Colorado Plateaus and Basin and Range provinces, *Geology*, *1*, 107–110, doi:10.1130/0091-7613(1973)1<107:AATTBT>2.0.CO;2.

Shuey, R. T., D. K. Schellinger, A. C. Tripp, and L. B. Alley (1977), Curie depth determination from aeromagnetic spectra, *Geophys. J. R. Astron. Soc.*, *50*, 75–101.

Simpson, F., and K. Bahr (2005), *Practical Magnetotellurics*, 254 pp., Cambridge Univ. Press, Cambridge, U. K.

Sims, P. K., and H. J. Stein (2003), Tectonic evolution of the Proterozoic Colorado province, Southern Rocky Mountains: A summary and appraisal, *Rocky Mt. Geol.*, *38*(2), 183–204, doi:10.2113/gsrocky.38.2.183.

Siripunvaraporn, W., G. Egbert, and M. Uyeshima (2005), Interpretation of two-dimensional magneto-telluric profile data with three-dimensional inversion: Synthetic examples, *Geophys. J. Int.*, *160*(3), 804–814, doi:10/1111j.1365-246X.

Smith, D., J. N. Connelly, K. Manser, D. E. Moser, T. B. Housh, F. W. McDowell, and L. E. Mack (2004), Evolution of Navajo eclogites and hydration of the mantle wedge below the Colorado Plateau, southwestern United States, *Geochem. Geophys. Geosyst.*, *5*, Q04005, doi:10.1029/2003GC000675.

Smith, E. I., A. Sanchez, J. D. Walker, and K. Wang (1999), Geochemistry of mafic magmas in the Hurricane Volcanic Field, Utah: Implications for small- and large-scale chemical variability of the lithospheric mantle, *J. Geol.*, *107*, 433–448, doi:10.1086/314355.

Smith, R. B., W. C. Nagy, K. A. S. Julander, J. J. Viveiros, C. A. Barker, and D. J. Gants (1989), Geophysical and tectonic framework of the eastern Basin and Range-Colorado Plateau-Rocky Mountain transition, in *Geophysical Framework of the Continental United States*, edited by L. C. Pakiser and W. D. Mooney, *Mem. Geol. Soc. Am.*, *172*, 205–233.

Sonder, L. J., and C. H. Jones (1999), Western United States: How the west was widened, *Annu. Rev. Earth Planet. Sci.*, *27*, 417–462, doi:10.1146/annurev.earth.27.1.417.

Speed, R., M. W. Elison, and F. R. Heck (1988), Phanerozoic tectonic evolution of the Great Basin, in *Metamorphism and Crustal Evolution of the Western United States*, Rubey vol. VII, edited by W. G. Ernst, pp. 572–605, Prentice-Hall, Englewood Cliffs, N. J.

Spencer, J. E. (1996), Uplift of the Colorado Plateau due to lithosphere attenuation during Laramide low-angle subduction, *J. Geophys. Res.*, *101*, 13,595–13,609, doi:10.1029/96JB00818.

Spiegelman, M. (2003), Linear analysis of melt band formation by simple shear, *Geochem. Geophys. Geosyst.*, *4*(9), 8615, doi:10.1029/2002GC000499.

Stewart, J. H. (1980), Geology of Nevada, *Spec. Publ. Nev. Bur. Mines Geol.*, *4*, 136 pp.

Stewart, J. H., W. J. Moore, and I. Zeitz (1977), East-west patterns of Cenozoic igneous rocks, aeromagnetic anomalies, and mineral deposits, Nevada and Utah, *Geol. Soc. Am. Bull.*, *88*, 67–77, doi:10.1130/0016-7606(1977)88<67:EPOCIR>2.0.CO;2.

Stewart, M. E., and W. J. Taylor (1996), Structural analysis and fault segment boundary identification along the Hurricane fault in southwestern Utah, *J. Struct. Geol.*, *18*, 1017–1029, doi:10.1016/0191-8141(96)00036-3.

Stockli, D. F., J. K. Linn, J. D. Walker, and T. A. Dumitru (2001), Miocene unroofing of the Canyon Range during extension along the Sevier Desert Detachment, west central Utah, *Tectonics*, *20*, 289–307.

Stodt, J. A. (1983), Conventional and remote reference processing of magnetotelluric data, Ph.D. thesis, 221 pp., Univ. of Utah, Salt Lake City.

Stokes, W. L. (1986), *Geology of Utah*, 280 pp., Utah Geol. Mineral. Surv, Salt Lake City.

Thatcher, W., and F. F. Pollitz (2008), Temporal evolution of continental lithospheric strength in actively deforming regions, *GSA Today*, *18*, 4–11, doi:10.1130/GSAT01804-5A.1.

Thompson, G. A., and M. L. Zoback (1979), Regional geophysics of the Colorado Plateau, *Tectonophysics*, *61*, 149–181, doi:10.1016/0040-1951(79)90296-8.

Thompson, R. N., D. Velde, P. T. Leat, M. A. Morrison, J. G. Mitchell, A. P. Dickin, and S. A. Gibson (1997), Oligocene lamproite containing an Al-poor, Ti-rich biotite, Middle Park, northwest Colorado, U.S.A., *Mineral. Mag.*, *61*, 557–572, doi:10.1180/minmag.1997.061.407.08.

Tingey, D. G., E. H. Christiansen, M. G. Best, J. Ruiz, and D. R. Lux (1991), Tertiary minette and melanepheline dikes, Wasatch Plateau, Utah: Records of mantle heterogeneities and changing tectonics, *J. Geophys. Res.*, *96*, 13,529–13,544, doi:10.1029/91JB00327.

Torres-Verdin, C., and F. X. Bostick, Jr. (1992), Principles of spatial surface electric field filtering in magnetotellurics: Electro-magnetic array profiling (EMAP), *Geophysics*, *57*, 603–622, doi:10.1190/1.1443273.

Tullis, J., R. A. Yund, and J. Farver (1996), Deformation-enhanced fluid distribution in feldspar aggregates and implications for ductile shear zones, *Geology*, *24*, 63–66, doi:10.1130/0091-7613(1996)024<0063:DEFDIF>2.3.CO;2.

Usui, T., E. Nakamura, and H. Helmstaedt (2006), Petrology and geochemistry of eclogite xenoliths from the Colorado Plateau: Implication for the evolution of subducted oceanic crust, *J. Petrol.*, *47*, 929–964, doi:10.1093/petrology/egi101.

Van Schmus, W. R., et al. (1993), Transcontinental Proterozoic provinces, in *The Geology of North America*, vol. C-2, *Precambrian: Coterminous U.S.*, edited by J. C. Reed , Jr. et al., pp. 171–334, Geol. Soc. of Am., Boulder, Colo.

Vauchez, A., A. Tommasi, G. Barruol, and J. Maumus (2000), Upper mantle deformation and seismic anisotropy in continental rifts, *Phys. Chem. Earth*, *25*, 111–117, doi:10.1016/S1464-1895(00)00019-3.

Vozoff, K. (1991), The magnetotelluric method, in *Electromagnetic Methods in Applied Geophysics*, vol. 2B, edited by M. N. Nabighian, pp. 641–711, Soc. of Explor. Geophys., Tulsa, Okla.

Walker, K. T., G. H. R. Bokelmann, and S. L. Klemperer (2004), Shear-wave splitting beneath the Snake River Plain suggests a mantle upwelling beneath eastern Nevada, USA, *Earth Planet. Sci. Lett.*, *222*, 529–542, doi:10.1016/j.epsl.2004.03.024.

Wang, D., M. Mookherjee, Y. Xu, and S. Karato (2006), The effect of water on the electrical conductivity of olivine, *Nature*, *443*, 977–980, doi:10.1038/nature05256.

Wannamaker, P. E. (1986), Electrical conductivity of water-undersaturated crustal melting, *J. Geophys. Res.*, *91*, 6321–6327, doi:10.1029/JB091iB06p06321.

Wannamaker, P. E. (1999), Affordable magnetotellurics: Interpretation in natural environments, in *Three-Dimensional Electromagnetics*, *Geophys. Dev. Ser.*, vol. 7, edited by M. Oristaglio and B. Spies, pp. 349–374, Soc. of Explor. Geophys., Tulsa, Okla.

Wannamaker, P. E. (2000), Comment on "The petrologic case for a dry lower crust" by B. D. Yardley and J. W. Valley, *J. Geophys. Res.*, *105*, 6057–6064, doi:10.1029/1999JB900324.

Wannamaker, P. E. (2005), Anisotropy versus heterogeneity in continental solid earth electro-magnetic studies: Fundamental response characteristics and implications for physico-chemical state, invited review paper, *Surv. Geophys.*, *26*, 733–765, doi:10.1007/s10712-005-1832-1.

Wannamaker, P. E., and G. W. Hohmann (1991), Electromagnetic induction studies, *U.S. Natl. Rep. Int. Union Geod. Geophys. 1987–1990, Rev. Geophys.*, *29*, 405–415.

Wannamaker, P. E., S. H. Ward, G. W. Hohmann, and W. R. Sill (1980), Magnetotelluric models of the Roosevelt Hot Springs thermal area, Utah, *U.S. Dept. Energy Rep. DOE/ET/27002-8*, 213 pp., Univ. of Utah, Salt Lake City.

Wannamaker, P. E., G. W. Hohmann, and S. H. Ward (1984), Magnetotelluric responses of three-dimensional bodies in layered earths, *Geophysics*, *49*, 1517–1534, doi:10.1190/1.1441777.

Wannamaker, P. E., J. A. Stodt, and L. Rijo (1987), A stable finite element solution for two-dimensional magnetotelluric modeling, *Geophys. J. R. Astron. Soc.*, *88*, 277–296.

Wannamaker, P. E., P. M. Wright, Z.-X. Zhou, X.-B. Li, and J.-X. Zhao (1991), Magnetotelluric transect of Long Valley caldera: Resistivity cross section, structural implications, and the limits of a two-dimensional analysis, *Geophysics*, *56*, 926–940, doi:10.1190/1.1443126.

Wannamaker, P. E., W. M. Doerner, J. A. Stodt, and J. M. Johnston (1997a), Subdued state of tectonism of the Great Basin interior relative to its eastern margin based on deep resistivity structure, *Earth Planet. Sci. Lett.*, *150*, 41–53, doi:10.1016/S0012-821X(97)00076-9.

Wannamaker, P. E., J. M. Johnston, J. A. Stodt, and J. R. Booker (1997b), Anatomy of the Southern Cordilleran Hingeline, Utah and Nevada, from deep resistivity profiling, *Geophysics*, *62*, 1069–1086, doi:10.1190/1.1444208.

Wannamaker, P. E., J. B. Hulen, and M. T. Heizler (2000), Early Miocene lamproite from the Colorado Plateau tectonic province, Utah, *J. Volcanol. Geotherm. Res.*, *96*, 176–191, doi:10.1016/S0377-0273(99)00146-8.

Wannamaker, P. E., et al. (2001), Great Basin-Colorado Plateau transition in central Utah: An interface between active extension and stable interior, in *The Geological Transition: Colorado Plateau to Basin and Range, Proceedings of the J. Hoover Mackin Symposium, Cedar City, Utah, September 20–23, UGA/AAPG Guideb. 30/GB78*, edited by M. C. Erskine et al., pp. 1–38, Utah Geol. Surv., Salt Lake City.

Wannamaker, P. E., G. R. Jiracek, J. A. Stodt, T. G. Caldwell, V. M. Gonzalez, J. D. McKnight, and A. D. Porter (2002), Fluid generation and pathways beneath an active compressional orogen, the New Zealand Southern Alps, inferred from magnetotelluric data, *J. Geophys. Res.*, *107*(B6), 2117, doi:10.1029/2001JB000186.

Wannamaker, P. E., P. E. Rose, W. M. Doerner, B. C. Berard, J. McCulloch, and K. Nurse (2004), Magnetotelluric surveying and monitoring at the Coso geothermal area, California, in support of the Enhanced Geothermal Systems concept: Survey parameters and initial results, paper SGP-TR-175 presented at Workshop on Geothermal Reservoir Engineering, Stanford University, Stanford, Calif.

Wannamaker, P. E., D. P. Hasterok, and W. M. Doerner (2006a), Possible magmatic input to the Dixie Valley geothermal field, and implications for district-scale resource exploration, inferred from magnetotelluric (MT) resistivity surveying, *Trans. Geotherm. Resour. Counc.*, *30*, 471–475.

Wannamaker, P. E., D. P. Hasterok, and W. M. Doerner (2006b), Possible magmatic input to the Dixie Valley geothermal field, Nevada, USA, with implications for district-scale resource exploration, inferred from MT surveying, extended abstract S7-O1 presented at 18th Biennial EM Induction in the Earth Symposium, El Vendrell, Spain, 17–23 Sept.

Wendlandt, E., D. J. Depaolo, and W. S. Baldridge (1993), Nd and Sr isotope chronostratigraphy of Colorado Plateau lithosphere: Implications for magmatic and tectonic underplating of the continental crust, *Earth Planet. Sci. Lett.*, *116*, 23–43, doi:10.1016/0012-821X(93)90043-9.

Wernicke, B. P. (1985), Uniform sense normal simple shear of the continental lithosphere, *Can. J. Earth Sci.*, *22*, 108–125.

Wernicke, B. (1992), Cenozoic extensional tectonics of the U.S. Cordillera, in *The Geology of North America*, vol. G-3, *The Cordilleran Orogen: Coterminous U.S.*, edited by B. C. Burchfiel, P. W. Lipman, and M. L. Zoback, pp. 553–581, Geol. Soc. of Am., Boulder, Colo.

Wernicke, B., and J. K. Snow (1998), Cenozoic tectonism in the central Basin and Range: Motion of the Sierran-Great Valley block, *Int. Geol. Rev.*, *40*, 403–410.

Wernicke, B., et al. (1996), Origin of high mountains in the continents: The southern Sierra Nevada, *Science*, *271*, 190–193, doi:10.1126/science.271.5246.190.

White, R., and D. McKenzie (1989), Magmatism at rift zones: The generation of volcanic continental margins and flood basalts, *J. Geophys. Res.*, *94*, 7685–7729, doi:10.1029/JB094iB06p07685.

Wills, S., M. H. Anders, and N. Christie-Blick (2005), Pattern of Mesozoic thrust surfaces and Tertiary normal faults in the Sevier Desert subsurface, west-central Utah, *Am. J. Sci.*, *305*, 42–100, doi:10.2475/ajs.305.1.42.

Wolf, L. W., and J. J. Cipar (1993), Through thick and thin: A new model for the Colorado Plateau from seismic refraction data from Pacific to Arizona crustal experiment, *J. Geophys. Res.*, *98*, 19,881–19,894, doi:10.1029/93JB02163.

Wong, I. G., and D. S. Chapman (1990), Deep intraplate earthquakes in the western United States and their relationship to lithospheric temperatures, *Bull. Seismol. Soc. Am.*, *80*, 589–599.

Wood, B. J., and D. Virgo (1989), Upper mantle oxidation state: Ferric iron contents of lherzolite spinels by ^{57}Fe Mössbauer spectroscopy and resultant oxygen fugacities, *Geochim. Cosmochim. Acta*, *53*, 1277–1291, doi:10.1016/0016-7037(89)90062-8.

Wyld, S. J. (2002), Structural evolution of a Mesozoic back-arc fold and thrust belt in the U.S. Cordillera, new evidence from northwestern Nevada, *Geol. Soc. Am. Bull.*, *114*, 1452–1486, doi:10.1130/0016-7606(2002)114<1452:SEOAMB>2.0.CO;2.

Yardley, B. W. D., and J. W. Valley (1997), The petrologic case for a dry lower crust, *J. Geophys. Res.*, *102*, 12,173–12,185, doi:10.1029/97JB00508.

Yoshino, T., T. Matsuzaki, S. Yamashita, and T. Katsura (2006), Hydrous olivine unable to account for conductivity anomaly at the top of the asthenosphere, *Nature*, *443*, 973–976, doi:10.1038/nature05223.

Yoshino, T., G. Manthilake, T. Matsuzaki, and T. Katsura (2008), Dry mantle transition zone inferred from the conductivity of wadsleyite and ringwoodite, *Nature*, *451*, 326–329, doi:10.1038/nature06427.

Zandt, G. (2003), The southern Sierra Nevada drip and the mantle wind direction beneath the southwestern United States, *Int. Geol. Rev.*, *45*, 213–224, doi:10.2747/0020-6814.45.3.213.